

Accepted Manuscript

Title: Improved numerical inversion methods for the recovery of bivariate distributions of polymer properties from 2D probability generating function domains

Author: Adriana Brandolin Ayslane Assini Balbuena Mariano Asteasuain



PII: S0098-1354(16)30237-X
DOI: <http://dx.doi.org/doi:10.1016/j.compchemeng.2016.07.017>
Reference: CACE 5518

To appear in: *Computers and Chemical Engineering*

Received date: 12-8-2015
Revised date: 8-7-2016
Accepted date: 12-7-2016

Please cite this article as: Brandolin, Adriana., Balbuena, Ayslane Assini., & Asteasuain, Mariano., Improved numerical inversion methods for the recovery of bivariate distributions of polymer properties from 2D probability generating function domains. *Computers and Chemical Engineering* <http://dx.doi.org/10.1016/j.compchemeng.2016.07.017>

This is a PDF file of an unedited manuscript that has been accepted for publication. As a service to our customers we are providing this early version of the manuscript. The manuscript will undergo copyediting, typesetting, and review of the resulting proof before it is published in its final form. Please note that during the production process errors may be discovered which could affect the content, and all legal disclaimers that apply to the journal pertain.

Improved Numerical Inversion Methods for the Recovery of Bivariate Distributions of Polymer Properties from 2D Probability Generating Function Domains.

Adriana Brandolin, Ayslane Assini Balbueno, Mariano Asteasuain*

Prof. A. Brandolin

abrandolin@plapiqui.edu.ar

Planta Piloto de Ingeniería Química (PLAPIQUI), Universidad Nacional del Sur – CONICET, Bahía Blanca, 8000, Argentina.

Mrs. Ayslane Assini Balbueno

ayslane.asini@gmail.com

Federal University of Viçosa

Centro, Viçosa, Minas Gerais, Brazil.

Prof. M. Asteasuain (Corresponding author)

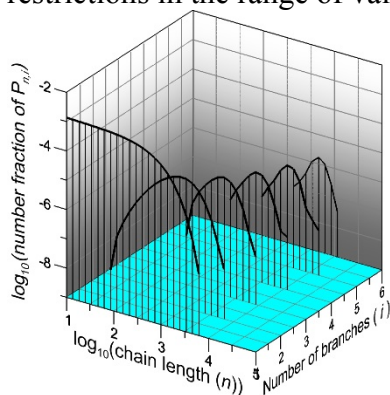
E-mail: masteasuain@plapiqui.edu.ar

Planta Piloto de Ingeniería Química (PLAPIQUI), Universidad Nacional del Sur – CONICET, Bahía Blanca, 8000, Argentina

TE: 54 291 4861700

GRAPHICAL ABSTRACT

In this work two 2D pgf inversion methods are developed, for which the pgf is regarded as a complex variable. These methods provide an outstanding accuracy in the inversion, thus allowing extending the 2D pgf technique for modeling bivariate distributions without restrictions in the range of values of its independent domains



HIGHLIGHTS

- Advanced modeling of polymer processes.
- Prediction of bivariate (2D) distributions of polymer molecular properties.
- Improvement of the pgf modeling method.
- Development of new pgf inversion methods that use complex and/or real pgf.
- Accurate modeling of 2D distributions with domains of different orders of magnitude.

Abstract

The 2D probability-generating function technique is a powerful method for modeling bivariate distributions of polymer properties. It is based on the transformation of bivariate population balance equations using 2D probability generating functions (pgf) followed by a recovery of the distributions from the transform domain by numerical inversion. A key step of this method is the inversion of the pgf transforms. Available numerical inversion methods yield excellent results for pgf transforms of distributions with independent dimensions with similar orders of magnitude, for example bivariate molecular weight distributions in copolymerization systems. However, numerical problems are found for 2D distributions in which the independent dimensions have very different ranges of values, such as the molecular weight distribution-branching distribution in branched polymers. In this work, two new 2D pgf inversion methods are developed, which regard the pgf as a complex variable. The superior accuracy of these innovative methods makes them suitable for recovering any type of bivariate distribution. This

enhances the capabilities of the 2D pgf modeling technique for simulation and optimization of polymer processes. An application example of the technique in a polymeric system of industrial interest is presented.

Keywords: modeling, polymerization, bivariate distribution, 2D probability generating function

1. Introduction

The microstructure of a polymer chain, which includes molecular weight distribution (MWD), copolymer composition distribution (CCD), long-chain branching distribution (LCBD), short-chain branching distribution (SCBD), sequence length distribution (SLD) etc., has a strong influence on the processing and end-use properties of the material (e.g., rheological, physical, chemical, mechanical, etc.). In many cases, a proper characterization of a polymer sample requires simultaneous information on the distributions of several properties. For example, joint information about both the molecular weight and chain composition distributions (MWD-CCD) is important for copolymer systems, while branched polymers require knowledge of their branching density and the molecular weight distribution (MWD-SCBD and/or MWD-LCBD). Operating the polymer processes with a focus on achieving tight control of the molecular architecture of the polymer chains is very important for polymer manufacturers. To this purpose, a thorough understanding of the complex relationships between the polymer synthesis conditions and the resulting molecular properties of the resin is very useful. Therefore, considerable effort has been devoted to developing detailed predictive models of polymer processes. The calculation of the distribution of a single property, in most cases the MWD, has been extensively studied. However, the treatment of more than one independent coordinate leads to highly complex problems for which very few solution approaches have been developed

One such approach is based on the solution of multivariate population balance equations (PBE). PBEs are drawn from a kinetic mechanism of the process, and they describe the evolution of the concentration of the different polymer species. However, the total number of equations commonly runs into the thousands. Consequently, the computational effort associated with the solution of the complete set of nonlinear balances is prohibitively high for most cases of interest. To deal with this high-dimensional problem, several numerical methods have been proposed in the literature.

One of these methods is the numerical fractionation technique. It was used for predicting the bivariate MWD-LBCD (Chen et al., 2015; Pladis & Kiparissides, 1998), the bivariate MWD-number of active sites distribution (Lazzari & Storti, 2014) and the single MWD of branched polymers (Kizilel et al., 2007; Papavasiliou & Teymour, 2003). It consists of dividing the total population of polymer chains into classes according to the number of branching points. Reconstruction of the MWD at high monomer conversions and high branching content may demand a high computational load because the number of classes required to reduce approximation errors is large.

In sectional methods (Singh et al., 2013), the distribution function is represented through population on a finite number of discrete pivots. One variant of this method, known as the Fixed Pivot Technique, keeps the pivots fixed in space and allows the evolution of the population on each pivot with time. This method has been applied to predict the MWD-CCD in copolymer systems (Krallis et al., 2008) and the MWD-LCBD in branched polymer systems (Butté et al., 2002; Meimaroglou et al., 2007). Although this method yields accurate results, it requires special computational skills to overcome its numerical complexity.

Additionally, Iedema et al. (2000) developed a calculus method based on the so-called distributed moments, in which the chain length distribution is calculated rigorously and the additional properties are computed as averages with respect to chain length. Iedema et al. (2013) also developed a method applicable to two-dimensional population problems based on

approximations of distributions in terms of Gaussian basis functions. This method is appropriate for problems where the evaluation of convolutions in both dimensions is crucial.

Recently, Zapata-González et al. (2011) solved the original system of PBEs, stating that this is possible only under certain circumstances. Although this technique involves dealing with a large system of equations, it is simple and straightforward to apply. This approach was used to predict the bivariate MWD of an intermediate moiety in RAFT polymerizations. The quasi-steady state approximation was used to remove the stiffness of the system of equations.

Another approach to modeling multivariate distributions is based on probabilistic methods. These are mainly represented by the Monte Carlo technique. This tool is relatively simple to apply and fits conveniently the discrete and stochastic nature of high-dimensional polymerization processes. It can also provide extremely detailed information about the polymer microstructure and the topological architecture of the chain that is not available with deterministic solvers. For example, Monte Carlo models have been used to predict the MWD-CCD in different copolymerization systems (Krallis et al., 2008; Ali Parsa et al., 2014), the MWD-LCBD in branched polymers (Costeux, 2003; Meimaroglou et al., 2007) and the MWD-LCBD-CCD of some polyolefins (Hamielec, 1997). A significant disadvantage of this technique is the high computational cost required to obtain accurate results, even with modern, parallelized systems (Wulkow, 2008).

Shütte and Wulkow (2010) presented a hybrid deterministic-stochastic method that combines some of the advantages of both approaches. This hybrid method is based on computing the basic chain length distribution deterministically and adding further properties using a stochastic method based on relatively small ensembles of chains. They applied this method to predict the bivariate MWD-CCD and trivariate MWD-CCD-LCBD in copolymerization systems.

In previous works (Asteasuain & Brandolin, 2010; Brandolin & Asteasuain, 2013) we presented a deterministic method for modeling bivariate distributions of polymer properties. It is based on the transformation of PBEs using 2D probability generating functions (pgf) followed by a

recovery of the distribution from the transform domain by numerical inversion. By means of a 2D pgf Transform Table, an easy transformation of any typical polymer balance equation can be achieved. This modeling technique can be used without resorting to any simplifying assumptions or a priori knowledge of the distribution shape. Besides, the pgf Transform Table allows an easy model formulation. The resulting model is usually composed by a DAE system of equations of a reasonable size that can be solved efficiently with standard computational resources.

A key step of this method is the inversion of the pgf transforms. Two inversion methods were developed (Asteasuain & Brandolin, 2010), which yielded excellent results for modeling the bivariate MWD in different copolymerization systems (Fortunatti et al., 2014; Gianoglio Pantano et al., 2011; Gianoglio Pantano et al., 2012). This joint distribution is characterized by two independent dimensions of similar orders of magnitude.

However, numerical problems were found when the pgf technique was applied to 2D distributions in which the independent dimensions had very different ranges of values. For example, in the MWD-SCBD or MWD-LCBD the molecular weight dimension typically varies between 1 and 10^5 or more, while the branching density normally ranges between 1 and 100. In some copolymer systems the MWD-CCD may also fall into this category, when the concentration of one of the comonomers in the polymer chains is very low (Abiko et al., 2015). In the present work, two new 2D pgf inversion methods are developed, which regard the pgf as a complex variable. These methods overcome the limitation presented by those described in our previous work (Asteasuain & Brandolin, 2010). The superior accuracy of these inversion methods makes them appropriate for recovering any type of bivariate distribution, which enhances the capabilities of the 2D pgf modeling technique. Thus this methodology becomes a powerful tool in the operation of polymer processes to aid the synthesis of polymers with pre-specified molecular architecture. An application example of the pgf method in a polymeric system of industrial interest is presented.

2. pgf inversion method

Modeling a bivariate distribution of polymer molecular properties involves calculating the concentration of the polymer chains $[P_{n,m}]$ for every possible value n and m of the two distributed properties. The pgf modeling technique is based on transforming the infinite set of mass balances of the polymer species $[P_{n,m}]$ to the pgf domain. Thus a finite set of balance equations for the pgf transform of the distribution is obtained. The pgf equations are solved and the original distribution is recovered by numerical inversion.

The 2D pgf transform is defined for a discrete bivariate probability distribution as follows:

$$\phi_{a_1, a_2}(z_1, z_2) = \sum_{n=0}^{\infty} \sum_{m=0}^{\infty} z_1^n z_2^m p_{a_1, a_2}(n, m) \quad (1)$$

In this expression, the random variables n and m are the distributed properties, and z_1 and z_2 are the dummy variables of the pgf corresponding to the transformation on the variables identified by n and m , respectively. The pgf order (a_1, a_2) is used to indicate different types of probabilities. The probability distribution $p_{a_1, a_2}(n, m)$ is related to the concentration of the chemical species by the following expression:

$$p_{a_1, a_2}(n, m) = \frac{n^{a_1} m^{a_2} [P_{n,m}]}{\sum_{r=0}^{\infty} \sum_{s=0}^{\infty} r^{a_1} s^{a_2} [P_{r,s}]} \quad (2)$$

The probability distribution has physical meaning for some combinations of (a_1, a_2) . For example, in the case of $a_1 = 0, a_2 = 0$ it is equivalent to the distribution of species P expressed as number fraction.

Replacing Eq. (2) into Eq. (1), the following expression for the pgf definition is obtained:

$$\phi_{a_1, a_2}(z_1, z_2) = \frac{1}{\sum_{r=0}^{\infty} \sum_{s=0}^{\infty} r^{a_1} s^{a_2} [P_{r,s}]} \sum_{n=0}^{\infty} \sum_{m=0}^{\infty} z_1^n z_2^m [P_{n,m}] = \frac{1}{\lambda_{a_1, a_2}} \sum_{n=0}^{\infty} \sum_{m=0}^{\infty} z_1^n z_2^m [P_{n,m}] \quad (3)$$

where $\lambda_{a_1, a_2} = \sum_{r=0}^{\infty} \sum_{s=0}^{\infty} r^{a_1} s^{a_2} [P_{r,s}]$ is the double moment of order (a_1, a_2) of the bivariate distribution of species P .

Once the pgf values are available, the original distribution function $p_{a_1, a_2}(n, m)$ can be recovered from its 2D pgf transform $\phi_{a_1, a_2}(z_1, z_2)$ by means of the double inversion:

$$p_{a_1, a_2}(n, m) = \Phi_{a_1, a_2}^{-2} \left\{ \phi_{a_1, a_2}(z_1, z_2) \right\} \quad (4)$$

Several methods have been proposed in the literature for the inversion of multivariate Laplace transforms (Abate et al., 1998; Brancik, 2002; Brančik, 2010; Chao et al., 2008; Singhal et al., 1975; Valkó & Abate, 2005; Xiao & Lee, 2006). In particular, Valkó & Abate (2005) used a two-step procedure in which the inversion is carried out stepwise in each independent dimension at a time, using univariate inversion methods in each of them. In this work, as in our previous reports, we applied this concept for the inversion of 2D pgf transforms, as explained below.

A two-step procedure is used in the development of the 2D inversion formulas. In the first step, z_1 is regarded as a constant and the inversion is performed with respect to z_2 only:

$$\hat{\phi}_{a_1, a_2}(z_1, m) = \Phi_{z_2}^{-1} \left\{ \phi_{a_1, a_2}(z_1, z_2) \right\} \quad (5)$$

In the second step, $\hat{\phi}_{a_1, a_2}(z_1, m)$ is inverted with respect to z_1 obtaining $p_{a_1, a_2}(n, m)$:

$$p_{a_1, a_2}(n, m) = \Phi_{z_1}^{-1} \left\{ \hat{\phi}_{a_1, a_2}(z_1, m) \right\} \quad (6)$$

Since inversion of univariate pgfs is performed in each of these steps, it is possible to use inversion algorithms developed for this type of pgf. Our previous 2D pgf inversion methods used inversion algorithms of real pgfs in each inversion step. However, the methods presented in this work use (in at least one of the inversion steps) a univariate pgf inversion method that regards the pgf as a complex function.

2.1 Inversion method of complex univariate pgfs

Different methods have been developed for the numerical inversion of complex univariate pgfs. Abate and Whitt (1992) and Abate et al. (2000) presented a Fourier-series method for the numerical inversion of pgfs. This method involves a discretization approach that requires a high number of pgf evaluations, which is not convenient for the inversion of pgf transforms of the MWD. The methods proposed by Cavers (1978) and Daigle (1989) use a different discretization approach, reducing the number of pgf evaluations. None of these authors applied their methods to the inversion of pgf in polymer systems. Mills (1986) developed a numerical inversion method of z-transforms with a similar approach to that of Cavers and Daigle to calculate polymer chain length distributions. It should be noted that the z-transform is a transform function that becomes equivalent to the pgf by an appropriate change of its dummy variable. Asteasuain (2003) developed a method for the numerical inversion of univariate pgfs similar to those mentioned above. In a similar way to Eq. (1), a univariate pgf was defined as

$$\phi(z) = \sum_{n=0}^{\infty} z^n p(n) \quad (7)$$

Substituting z in Equation (7) for the expression

$$z = e^{i\theta} = \cos(\theta) + i \sin(\theta), \quad (8)$$

that is, with z lying on the unit circle in the complex z -plane, gives

$$\phi(e^{i\theta}) = \sum_{n=0}^{\infty} \cos(n\theta) p(n) + i \sum_{n=0}^{\infty} \sin(n\theta) p(n) \quad (9)$$

Equation (9) allows identifying the real part ($f_r(\theta)$) and the imaginary part ($f_i(\theta)$) of $\phi(z)$:

$$f_r(\theta) = \sum_{n=0}^{\infty} \cos(n\theta) p(n) \quad (10)$$

$$f_i(\theta) = \sum_{n=0}^{\infty} \sin(n\theta) p(n) \quad (11)$$

Since $f_r(\theta)$ and $f_i(\theta)$ are even and odd functions of θ , respectively, they have expansions in cosine and sine Fourier series:

$$f_r(\theta) = \sum_{n=0}^{\infty} \cos(n\theta) a(n) \quad (12)$$

$$f_i(\theta) = \sum_{n=0}^{\infty} \sin(n\theta) a(n) \quad (13)$$

where $a(n)$ and $b(n)$ are the coefficients of the cosine and sine expansions, respectively. Comparing Eq. (10) with Eq. (12), and Eq. (11) with Eq. (13), it can be observed that the distribution $p(n)$ is equal to the coefficients of the cosine expansion of $f_r(\theta)$ and of the sine expansion of $f_i(\theta)$. Hence, it is possible to use the formulas for the coefficients of the Fourier series in order to obtain $p(n)$ from $f_r(\theta)$ or from $f_i(\theta)$:

$$p(n) = \frac{1}{\pi} \int_0^{2\pi} f_r(\theta) \cos(n\theta) d\theta = \frac{1}{\pi} \int_0^{2\pi} f_i(\theta) \sin(n\theta) d\theta \quad (14)$$

Combining both integrals of Eq. (14), an alternative formula for $p(n)$ can be obtained:

$$\begin{aligned} p(n) &= \frac{1}{2\pi} \int_0^{2\pi} (f_r(\theta) \cos(n\theta) + f_i(\theta) \sin(n\theta)) d\theta \\ &= \frac{1}{2\pi} \int_0^{2\pi} \Re(\phi(e^{i\theta}) e^{-in\theta}) d\theta \\ &= \frac{1}{2\pi} \int_0^{2\pi} \phi(e^{i\theta}) e^{-in\theta} d\theta \end{aligned} \quad (15)$$

These integrals can be approximated using the trapezoidal rule. This rule has been used by several authors for solving similar integrals, and has been proven to yield a smaller discretization error than other methods, such as Simpson's rule (Abate et al., 1998; Cavers, 1978; Daigle, 1989).

Approximating the integral of Eq. (15) with the trapezoidal method using $\Delta\theta = 2\pi/N$ gives the following inversion formula:

$$\begin{aligned}
p(n) \cong \bar{p}(n) &= \frac{1}{N} \left(\sum_{j=0}^{N-1} f_r \left(j \frac{2\pi}{N} \right) \cos \left(nj \frac{2\pi}{N} \right) + f_i \left(j \frac{2\pi}{N} \right) \sin \left(nj \frac{2\pi}{N} \right) \right) \\
&= \frac{1}{N} \left(\sum_{j=0}^{N-1} \phi \left(e^{j \frac{2\pi}{N}} \right) e^{-inj \frac{2\pi}{N}} \right)
\end{aligned} \tag{16}$$

where $\bar{p}(n)$ is the approximation of the true distribution $p(n)$.

Other similar expressions can be obtained for the integrals in Eq. (14). However, the expression in Eq. (16) has a smaller truncation error due to cancellation of some of the error terms that are present in the alternative formulas (Asteasuain, 2003). Relevant properties of the inversion formula of Eq. (16) are described below. Firstly, the inversion formula is valid for $n \leq N-1$, since it yields:

$$\bar{p}(kN + n) = \bar{p}(n), \quad k = 1, 2, \dots \tag{17}$$

This means that the formula is periodic with period N . Therefore, values calculated for $n \geq N$ bear no relation to the true values of the distribution.

Another important feature is the number of pgf evaluations required. According to Eq. (16), this value is equal to N . However, due to symmetry properties of the pgf with respect to θ (Asteasuain, 2003):

$$\begin{aligned}
f_r \left((N-j) \frac{2\pi}{N} \right) &= f_r \left(j \frac{2\pi}{N} \right) \\
f_i \left((N-j) \frac{2\pi}{N} \right) &= -f_i \left(j \frac{2\pi}{N} \right)
\end{aligned} \tag{18}$$

the number of function evaluations is reduced to $N/2$. Therefore, parameter N both limits the range of applicability of the inversion formula and determines the number of function evaluations. Although small values of N would reduce the number of pgf evaluations, there is a constraint due to the relationship between N and the inversion error. It can be demonstrated that the error of the method is (Asteasuain, 2003):

$$e(n) = \bar{p}(n) - p(n) = \sum_{k=1}^{\infty} p(kN + n) \tag{19}$$

This means that the distribution recovered for $n \leq N - 1$ consists of the actual distribution points in this interval plus the sum of the curve segments in the intervals $kN \leq n \leq 2kN - 1$, $k = 1, \dots, \infty$. For example, for $N = 100$, the recovered distribution $\bar{p}(n)$ for $1 \leq n \leq 99$ is equal to the actual distribution $p(n)$ in that interval (desired result), plus the actual distribution in the interval $100 \leq n \leq 199$, plus the actual distribution in the interval $200 \leq n \leq 299$, etc. (i.e. $\bar{p}(5) - p(5) = p(105) + p(205) + \dots + p(5 + k \cdot 100)$). This error cannot be evaluated without knowledge of the true distribution. However, it can be observed that the inversion error becomes negligible by setting N to a value larger than the maximum significant value of the independent distributed variable, i.e. by setting N such that $p(n) \approx 0$ for $n \geq N$. From the point of view of a user of the method, the latter is a key property. It means that the whole bell of the distribution should be included in the interval $[0, N]$ for the error to be insignificant, otherwise the computed distribution is likely to be inaccurate. Another important property is that the inversion formula of Eq. (16) is not valid for n values beyond N , as shown by Eq. (17).

2.2 Inversion methods of 2D pgfs

Two inversion methods of 2D pgfs will now be presented. The first one uses the univariate pgf inversion method described above (called IFG method from now on) for both steps of the 2D pgf inversion (see Eq. (5) and (6)). The second method uses IFG in the first step and an inversion method of the real univariate pgfs in the second step.

2.2.1 2D IFG method

In this method the inversion formula given in Eq. (16) is used in the two inversion steps. Applying it in the first step described in Eq. (5) yields

$$\hat{\phi}_{a_1, a_2}(z_1, m) = \frac{1}{N_2} \sum_{j_2=0}^{N_2-1} \left(\phi_{a_1, a_2} \left(z_1, e^{ij_2 \frac{2\pi}{N_2}} \right) e^{-imj_2 \frac{2\pi}{N_2}} \right) \quad (20)$$

When the IFG formula is applied in the second inversion step given by Eq. (6), the following expression is obtained:

$$\bar{p}_{a_1, a_2}(n, m) = \frac{1}{N_1} \sum_{j_1=0}^{N_1-1} \left(\hat{\phi}_{a_1, a_2} \left(e^{j_1 \frac{2\pi}{N_1}}, m \right) e^{-imj_1 \frac{2\pi}{N_1}} \right) \quad (21)$$

Substituting Eq. (20) into Eq. (21) with $z_1 = e^{j_1 \frac{2\pi}{N_1}}$ gives

$$\begin{aligned} \bar{p}_{a_1, a_2}(n, m) &= \frac{1}{N_1} \sum_{j_1=0}^{N_1-1} \left(\frac{1}{N_2} \sum_{j_2=0}^{N_2-1} \left(\phi_{a_1, a_2} \left(e^{j_1 \frac{2\pi}{N_1}}, e^{j_2 \frac{2\pi}{N_2}} \right) e^{-imj_2 \frac{2\pi}{N_2}} \right) e^{-imj_1 \frac{2\pi}{N_1}} \right) \\ &= \frac{1}{N_1 N_2} \sum_{j_1=0}^{N_1-1} \sum_{j_2=0}^{N_2-1} \left(\phi_{a_1, a_2} \left(e^{j_1 \frac{2\pi}{N_1}}, e^{j_2 \frac{2\pi}{N_2}} \right) e^{-i \left(nj_1 \frac{2\pi}{N_1} + mj_2 \frac{2\pi}{N_2} \right)} \right) \\ &= \frac{1}{N_1 N_2} \sum_{j_1=0}^{N_1-1} \sum_{j_2=0}^{N_2-1} \left(\begin{aligned} &f_r \left(j_1 \frac{2\pi}{N_1}, j_2 \frac{2\pi}{N_2} \right) \cos \left(nj_1 \frac{2\pi}{N_1} + mj_2 \frac{2\pi}{N_2} \right) \\ &+ f_i \left(j_1 \frac{2\pi}{N_1}, j_2 \frac{2\pi}{N_2} \right) \sin \left(nj_1 \frac{2\pi}{N_1} + mj_2 \frac{2\pi}{N_2} \right) \end{aligned} \right) \end{aligned} \quad (22)$$

In this equation, $f_r(\theta_1, \theta_2)$ and $f_i(\theta_1, \theta_2)$ are the real and imaginary parts, respectively, of $\phi_{a_1, a_2}(e^{i\theta_1}, e^{i\theta_2})$. In order to achieve good accuracy, the constraint on the value of parameter N described in the previous section has to be extended to each dimension involved in the inversion formula of the 2D IFG method (Eq. (22)). This implies that parameters N_1 and N_2 have to be larger than the maximum significant values in the dimensions of n and m , respectively. In addition, the required total number of pgf evaluations n_{ev} is in principle $n_{ev} = N_1 N_2$. However, for the bivariate pgf the following symmetry relationships can be obtained:

$$f_r \left((N_1 - j_1) \frac{2\pi}{N_1}, (N_2 - j_2) \frac{2\pi}{N_2} \right) = f_r \left(j_1 \frac{2\pi}{N_1}, j_2 \frac{2\pi}{N_2} \right) \quad (23)$$

$$f_i \left((N_1 - j_1) \frac{2\pi}{N_1}, (N_2 - j_2) \frac{2\pi}{N_2} \right) = -f_i \left(j_1 \frac{2\pi}{N_1}, j_2 \frac{2\pi}{N_2} \right) \quad (24)$$

These symmetry properties allow reducing the pgf evaluations to

$$n_{ev} = N_1 + (N_2 - 1) \left(\frac{N_1}{2} + 1 \right) = \frac{N_1 N_2}{2} + N_2 + \frac{N_1}{2} - 1. \text{^a This number may become considerably$$

large if at least one of the distributed properties is the molecular weight, whose significant range may easily reach values of order 10^5 or more. It should be noted that the number of function evaluations does not depend on the points (n, m) for which the distribution $p(n, m)$ is to be recovered, but only on parameters N_1 and N_2 .

An expression for the inversion error of this method can be obtained by applying twice the error of the univariate IFG shown in Eq. (19), once to each of the two independent dimensions. The resulting error expression for the 2D IFG method is

$$e(n, m) = \bar{p}(n, m) - p(n, m) = \sum_{k=1}^{\infty} p(n + kN_1, m) + \sum_{k=1}^{\infty} p(n, m + kN_2) + \sum_{k=1}^{\infty} \sum_{l=1}^{\infty} p(n + kN_1, m + lN_2) \quad (25)$$

As discussed for the univariate IFG, the inversion error is made negligible by selecting N_1 and N_2 values large enough so that $p(n, N_2), p(N_1, m) \approx 0 \quad \forall n, m$. Note that, since the distribution $p(n, m) \geq 0$, the inversion error is always nonnegative.

2.2.2 2D PAP-IFG method

This method applies the IFG formula in one of the inversion steps, and an inversion method for real pgfs in the second one. The latter is an adaptation of the Papoulis inversion method of Laplace transforms to pgf (PAP method from now on) that we developed and applied in our

^a The 2D IFG method requires pgf values at a number of (z_1, z_2) points with $z_1 = e^{ij_1 \frac{2\pi}{N_1}}$ and $z_2 = e^{ij_2 \frac{2\pi}{N_2}}$, where $j_1 = 0, \dots, N_1 - 1$ and $j_2 = 0, \dots, N_2 - 1$. This expression for n_{ev} results from considering that the pgf is calculated for $j_2 = 0, \dots, N_2 - 1$ and $j_1 = 0, \dots, N_1/2$, and that the remaining points are obtained by applying the symmetry properties. Alternatively, the pgf may be calculated for $j_1 = 0, \dots, N_1 - 1$ and $j_2 = 0, \dots, N_2/2$ with the remaining pgf values being obtained by symmetry. In this case the number of pgf evaluations would be $n_{ev} = \frac{N_1 N_2}{2} + N_1 + \frac{N_2}{2} - 1$. These two possibilities for n_{ev} differ in the second and third terms, which are considerably smaller than the first one. According to the relative values of N_1 and N_2 , any of the two options may be chosen by the user in order to reduce (slightly) the number of pgf evaluations.

previous 2D pgf inversion methods (Asteasuain & Brandolin, 2010). The modified Papoulis inversion formula is

$$\bar{p}(n) = (\mathbf{b}(n))^T \cdot \mathbf{v} = \sum_{j_1=0}^{N_p} b(n)_{j_1} v_{j_1} \quad (26)$$

where \mathbf{v} is a vector defined by

$$\mathbf{v} = (\mathbf{A}^{-1})^T \cdot \mathbf{L}_{2N}(1/2) \quad (27)$$

In this expression, \mathbf{A} is the lower triangular matrix whose elements $A_{i,j}$ are

$$A_{i,j} = \frac{(i-j+1)_j}{2(i+1/2)_{j+1}} \quad j=0, \dots, i \text{ and } i=0, \dots, N_p \quad (28)$$

The expressions in the numerator and denominator of this equations, $(i-j+1)_j$ and $(i+1/2)_{j+1}$, are calculated as follows: Let f be the expression between parentheses and h the subscript, then $(f)_h$ is

$$(f)_h = \begin{cases} 1 & h=0 \\ f(f+1)\dots(f+h-1) & h>0 \end{cases} \quad (29)$$

The variable \mathbf{L}_{2N} in Eq. (27) is a vector whose elements $L_{2N,j}$, $j=0, \dots, N_p$ are Legendre polynomials of order $2j$ evaluated at $x=1/2$. Legendre polynomials are calculated as follows:

$$\begin{aligned} L_0(x) &= 1 \\ L_1(x) &= x \\ &\vdots \\ (l+1)L_{l+1}(x) &= (2l+1)xL_l(x) + lL_{l-1}(x) \end{aligned} \quad (30)$$

Pgf transforms are found in vector $\mathbf{b}(n)$, which is defined by

$$b(n)_i = \frac{\ln(2)}{n} \phi \left(e^{-\frac{(2i+1)\ln(2)}{n}} \right) \quad i=0, \dots, N_p \quad (31)$$

Including the PAP formula into Eq. (6), which corresponds to the second inversion step, yields the following expression:

$$\bar{p}_{a_1, a_2}(n, m) = \frac{\ln(2)}{n} \sum_{j_1=0}^{N_p} \left(\hat{\phi}_{a_1, a_2} \left(e^{\frac{(2j_1+1)\ln(2)}{n}}, m \right) v_{j_1} \right) \quad (32)$$

As with the 2D IFG method, $\hat{\phi}_{a_1, a_2}(z1, m)$, $z1 = e^{\frac{(2j_1+1)\ln(2)}{n}}$ (real) is computed using the IFG formula for the first inversion step (Eq. (20)). Thus the inversion formula of the 2D PAP-IFG method is obtained:

$$\begin{aligned} \bar{p}_{a_1, a_2}(n, m) &= \frac{\ln(2)}{n} \sum_{j_1=0}^{N_p} \left(\left(\frac{1}{N_2} \sum_{j_2=0}^{N_2-1} \left(\phi_{a_1, a_2} \left(e^{\frac{(2j_1+1)\ln(2)}{n}}, e^{ij_2 \frac{2\pi}{N_2}} \right) e^{-imj_2 \frac{2\pi}{N_2}} \right) \right) v_{j_1} \right) \\ &= \frac{\ln(2)}{nN_2} \sum_{j_1=0}^{N_p} \sum_{j_2=0}^{N_2-1} \left(\phi_{a_1, a_2} \left(e^{\frac{(2j_1+1)\ln(2)}{n}}, e^{ij_2 \frac{2\pi}{N_2}} \right) e^{-imj_2 \frac{2\pi}{N_2}} v_{j_1} \right) \\ &= \frac{\ln(2)}{nN_2} \sum_{j_1=0}^{N_p} \sum_{j_2=0}^{N_2-1} \left(\begin{aligned} &f_r \left(e^{\frac{(2j_1+1)\ln(2)}{n}}, e^{ij_2 \frac{2\pi}{N_2}} \right) \cos \left(mj_2 \frac{2\pi}{N_2} \right) v_{j_1} \\ &+ f_i \left(e^{\frac{(2j_1+1)\ln(2)}{n}}, e^{ij_2 \frac{2\pi}{N_2}} \right) \sin \left(mj_2 \frac{2\pi}{N_2} \right) v_{j_1} \end{aligned} \right) \end{aligned} \quad (33)$$

In the case of the 2D IFG method, ϕ_{a_1, a_2} is a complex function whose independent variables ($z1$ and $z2$) are both complex. In the 2D PAP-IFG method, ϕ_{a_1, a_2} is a complex function with $z1$ real and $z2$ complex. In Eq. (33), $f_r(z1, \theta_2)$ and $f_i(z1, \theta_2)$ are the real and imaginary parts of $\phi_{a_1, a_2}(z1, e^{i\theta_2})$, respectively. The 2D PAP-IFG method has two parameters: N_p and N_2 . As for the 2D IFG method, these parameters influence the inversion error and the number of pgf evaluations.

Unlike the 2D IFG method, it is not possible to develop an expression for the inversion error for the 2D PAP-IFG method, because no error formula is available for the univariate Papoulis method. However, some guidelines can be indicated. Firstly, parameter N_2 needs to be larger than the maximum significant value in the dimension of m in order to make the error of the inversion in this dimension negligible, as discussed above. As for parameter N_p , it represents the number of terms in a polynomial expansion in the dimension of n of the original distribution.

Large values reduce the truncation error, but increase the round-off error at the same time. Therefore, there is an optimum value that minimizes the total error, and this value can be found by convergence of the distributions recovered with successive values of this parameter. Usually, optimum values are about $N_P = 10-20$. More details can be found elsewhere (Asteasuain & Brandolin, 2010).

Parameters N_P and N_2 also determine the number of pgf evaluations. As observed in Eq. (33), $\phi_{a_1, a_2}(z_1, z_2)$ is evaluated at a set of values (z_{1i}, z_{2j}) for which $z_{2j}, j = 0, \dots, N_2$ depends only on parameter N_2 ; alternatively, $z_{1i}, i = 0, \dots, N_P$ depends on both N_P (which determines the number of z_1 values) and on the value of n for which the distribution $p(n, m)$ is to be required. The total number of pgf evaluations required by the PAP-IFG method is $n_{ev} = N_n (N_P + 1) \left(\frac{N_2}{2} + 1 \right)$,

where N_n is the number of values of n for which the distribution will be computed. The number of pgf evaluations n_{ev} takes into account the symmetry properties of the complex pgf:

$$f_r \left(e^{-\frac{(2j_1+1)\ln(2)}{n}}, (N_2 - j_2) \frac{2\pi}{N_2} \right) = f_r \left(e^{-\frac{(2j_1+1)\ln(2)}{n}}, j_2 \frac{2\pi}{N_2} \right) \quad (34)$$

$$f_i \left(e^{-\frac{(2j_1+1)\ln(2)}{n}}, (N_2 - j_2) \frac{2\pi}{N_2} \right) = -f_i \left(e^{-\frac{(2j_1+1)\ln(2)}{n}}, j_2 \frac{2\pi}{N_2} \right) \quad (35)$$

Since the optimal value of parameter N_P is not related at all with the range of values of the variable n , it is convenient to assign this domain to the distributed property with the largest order of magnitude. The number of calculated points in the domain of n (N_n) is a user-defined parameter that only determines the desired level of detail in the predicted distribution.

Both inversion methods (2D IFG and 2D PAP-IFG) will be first tested against the inversion of 2D pgf of bivariate distributions with known pgf transforms. Then an example of an actual polymeric system in which the polymer is characterized by a bivariate distribution with domains of different orders of magnitude will be presented. In this example, the 2D pgf technique is used

to predict the bivariate MWD-BD for a polyethylene produced by a mixed metallocene catalyst system.

3. Results and Discussion

3.1 Performance of the 2D pgf inversion methods. Recovery of distributions with known pgf transforms

Bivariate distributions for which the analytical expression of their pgf transforms is known were initially used to test the inversion methods. Distributions with known pgf transforms were selected so as to avoid any contribution of the pgf value to the error in the recovered distribution (i.e. a pgf obtained by numerical solution of balance equations may be corrupted by numerical noise). The following analytical distributions were used:

$$p^1(n, m) = \frac{\mu_1^n e^{-\mu_1}}{n!} \frac{\mu_2^m e^{-\mu_2}}{m!} \quad (36)$$

$$p^2(n, m) = n(1-q)^2 q^{n-1} \frac{\mu^m e^{-\mu}}{m!} \quad (37)$$

These distributions were selected because their shape resembles that of distributions that can be found in polymer systems, and their pgf transforms are known. These pgf transforms are:

$$\phi^1(z_1, z_2) = e^{(z_1-1)\mu_1 + (z_2-1)\mu_2} \quad (38)$$

$$\phi^2(z_1, z_2) = \frac{(1-q)^2 z_1 e^{(z_2-1)\mu}}{(1-z_1q)^2} \quad (39)$$

The values of the parameters of distributions $p^1(n, m)$ and $p^2(n, m)$ were set at $\mu_1 = 100$, $\mu_2 = 5$, and $q = 0.999$, $\mu = 5$, respectively. These values were chosen so that the distributions would result in independent variables with very different ranges of values. **Figures 1** and **2** show the results obtained for the 2D IFG method. It can be observed that an outstanding accuracy was obtained. The pgf inversion was carried out with $N_1 = 140$, $N_2 = 16$ for $p^1(n, m)$,

and $N_1 = 8000$, $N_2 = 20$ for $p^2(n, m)$. The number of pgf evaluations was 1120 in the first case and 80 000 in the second case.

As mentioned in section 2.2.1, parameters N_1 and N_2 should be set to values large enough so that $p(n, N_2), p(N_1, m) \approx 0 \quad \forall n, m$ in order to ensure a negligible inversion error. It can be inferred from the graphs in Figs. 1 and 2 that the set of (N_1, N_2) values chosen for each distribution fulfils this requirement. As a result, the inversion error in both cases is insignificant. It should be noted that the values of N_1 and N_2 are conservative regarding the error requirement. Lower values could also have been used with small inversion error. Parameters N_1 and N_2 cannot be set if the approximate range of the distribution is not known in advance, but a few preliminary simulations are sufficient to determine the required information. The user would benefit from understanding in detail how the parameter values influence the inversion error. For this reason, an example of the sensitivity of the error of the inversion method with respect to the values of N_1 and N_2 is included in the Appendix section.

The two bivariate distributions recovered with the 2D PAP-IFG method are shown in **Figs. 3 and 4**.

A very good level of accuracy in the inversion was also obtained in this case. The parameters were $N_p = 30$, $N_2 = 16$ in the case of $p^1(n, m)$, and $N_p = 12$, $N_2 = 20$ for $p^2(n, m)$.

As discussed above, the influence of parameter N_2 on the inversion error is very similar in both methods (2D IFG and 2D PAP-IFG). Therefore, the error in the inversion in the dimension of m is made negligible by selecting a sufficiently large value of N_2 .

An appropriate value of parameter N_p results from a trade-off between truncation and round-off errors. This value can be obtained by seeking for the convergence of the recovered distributions when increasing N_p . An example of this procedure is shown in the Appendix. As discussed in the Appendix, the Papoulis method cannot guarantee accuracy in the inversion (in the dimension of n in this case). However, experience shows that a good convergence of the

distributions when finding the value of N_p is correlated with good accuracy in the inversion, as was the case in these examples.

The number of points in the n domain for the first and second distributions were 31 and 21 points, respectively. For these conditions, the number of pgf evaluations in each case was 8649 and 2730. Therefore, the 2D IFG method is more appropriate for the first distribution, but the 2D PAP-IFG method is better for the second one. In fact, only 2 seconds are needed in a standard desktop computer to compute $p^2(n, m)$ with the 2D PAP-IFG method, whereas almost 30 minutes are necessary with the 2D IFG method. This means that, from the point of view of computational effort, balance shifts from 2D IFG to 2D PAP-IFG as the size of the n domain grows.

3.2 Modeling of bivariate distributions in polymer systems

This section illustrates the use of the pgf technique for modeling bivariate distributions with domains of different orders of magnitude in polymer systems. The case study involves the prediction of the MWD-LCBD of a polyethylene produced by a mixed metallocene catalyst system in a continuous stirred-tank reactor (CSTR) and a semibatch reactor. This type of branched polyethylene synthesized by metallocene catalysts, known as mLLDPE, is industrially produced by Dow and other chemical companies. This polymer, which contains LCB in its chain structure, competes with LDPE in some applications. Recently, Dow introduced a new metallocene polymerization process that allows greater flexibility in tailoring molecular weight distribution, SCBD and LCBD specific to an application's requirements. It gives the manufacturer greater freedom in designing resins and meeting ongoing demands of polyethylene films. This development led to the mLLDPE ELITE™ series of polyethylenes (Dow Polyethylene, 2011).

In general, the rheological behavior of branched polymers differs from that of their linear counterparts. The flow properties of branched chains depend strongly on the molecular architecture, in particular on the type and number of long-chain branches. For this reason, a deep understanding of the relationship between the rheological properties of the material and the synthesis conditions is an essential issue for developers. One of the key components of this relationship is the connection between the synthesis conditions and the bivariate MWD-LCBD of the polymer. The latter is an input to advanced rheological models that can predict the melt flow properties of the resin (Pladis et al., 2015).

The process under consideration is specifically the polymerization of ethylene under the mixed metallocene catalyst system $\text{Et}[\text{Ind}]_2\text{ZrCl}_2/\text{CGC-Ti}$. Catalyst type 1 (constrained geometry catalyst, CGC-Ti) is capable of polymerizing both monomers and macromonomers (incorporating long-chain branches), whereas catalyst type 2 (linear catalyst, $\text{Et}[\text{Ind}]_2\text{ZrCl}_2$) can only polymerize monomers (unable to incorporate macromonomers). A generally accepted kinetic mechanism (Iedema & Hoefsloot, 2003) is presented in **Table 1**.

In these kinetic equations, $R_{n,i}^b$ is a growing polymer radical on a CGC-Ti catalyst with chain length n and i branches, $R_{n,1}^{\text{lin}}$ is a linear growing polymer radical on an $\text{Et}[\text{Ind}]_2\text{ZrCl}_2$ catalyst with chain length n , $P_{n,i}^{\text{b=}}$ and $P_{n,i}^{\text{b}}$ are dead polymer chains with chain length n and i branches from a CGC-Ti catalyst, with and without a terminal double bond, respectively, and $P_{n,1}^{\text{lin=}}$ and $P_{n,1}^{\text{lin}}$ are linear dead polymer chains with chain length n from an $\text{Et}[\text{Ind}]_2\text{ZrCl}_2$ catalyst, with and without a terminal double bond, respectively. It is worth mentioning that the total concentration of dead polymer chains with a terminal double bond is $P_{n,i}^{\text{=}} = P_{n,i}^{\text{b=}} + P_{n,i}^{\text{lin=}}$. The main polymer chain is taken as a branch, for example $P_{n,1}^{\text{b}}$ is a linear dead polymer chain from a CGC-Ti catalyst. The values assigned to the kinetic constants (Iedema & Hoefsloot, 2003) are shown in **Table 2**.

Notice that branched molecules are formed by the terminal double bond propagation on a CGC-Ti catalyst, in which macromonomers are incorporated into growing chains. Dead chains with a terminal double bond (macromonomers) are generated at both linear and branching catalysts in β -hydride elimination, transfer to monomer and catalyst deactivation reactions.

Population balances for a steady-state CSTR drawn from this kinetic mechanism are shown in **Table 3**. In the case of a batch reactor, the left-hand side of these balances should be changed for the derivatives of the species with respect to time. At the same time, the last term on the right-hand side does not appear because it corresponds to the inlet and outlet streams.

The model assumes instantaneous activation, and so balances for the activated catalysts (C_{CGC}^* and C_{lin}^*) can be solved using the initial catalyst concentrations as the initial values for the activated catalyst concentrations. The model also considers constant monomer concentration. Therefore, the CSTR balances are valid for steady-state operation, and the batch reactor balances represent the usual constant monomer pressure operating strategy of a semibatch reactor (Iedema & Hoefsloot, 2003). As a consequence of this assumption, the multiplication of propagation constants by monomer concentration can be considered a constant value, as reported in **Table 2**.

Some of the population balances of the polymer species are functions of zero order moments

of the polymeric species distributions of $R_{n,i}^b$, $R_{n,1}^{lin}$ and $P_{n,i}^-$ ($\lambda_{0,0}^b = \sum_{n=1}^{\infty} \sum_{i=1}^{\infty} [R_{n,i}^b]$, $\lambda_0^{lin} = \sum_{n=1}^{\infty} [R_{n,1}^{lin}]$

and $\mu_{0,0}^- = \sum_{n=1}^{\infty} \sum_{i=1}^{\infty} [P_{n,i}^-]$). Since $P_{n,i}^- = P_{n,i}^{b=} + P_{n,i}^{lin=}$ and $P_{n,i}^{lin=} = 0$ for $i=2, \dots, \infty$, $\mu_{0,0}^-$ can be computed

as $\mu_{0,0}^- = \sum_{n=1}^{\infty} \sum_{i=1}^{\infty} ([P_{n,i}^{b=}] + [P_{n,i}^{lin=}]) = \sum_{n=1}^{\infty} \sum_{i=1}^{\infty} [P_{n,i}^{b=}] + \sum_{n=1}^{\infty} [P_{n,1}^{lin=}] = \mu_{0,0}^{b=} + \mu_0^{lin=}$. It will also be necessary

to define zero order moments of the distributions of $P_{n,i}^b$ ($\mu_{0,0}^b = \sum_{n=1}^{\infty} \sum_{i=1}^{\infty} [P_{n,i}^b]$) and $P_{n,1}^{lin}$

($\mu_0^{lin} = \sum_{n=1}^{\infty} [P_{n,1}^{lin}]$).

The first step in the pgf modeling technique is to transform the balance equations of the polymeric species (Eq. (42)-(47)) into the pgf domain, obtaining balance equations for the pgfs of the polymer species distributions. The distributions of $R_{n,i}^b$, $P_{n,i}^{b=}$ and $P_{n,i}^b$ are bivariate, leading to 2D pgfs. On the other hand, the distributions of $R_{n,1}^{lin}$, $P_{n,1}^{lin=}$ and $P_{n,1}^{lin}$ are univariate since these are linear chains, resulting in univariate pgfs. The transformation of the balance equations can be carried out without difficulty by applying 2D pgf (Brandolin & Asteasuain, 2013) and 1D pgf (Asteasuain et al., 2002) transform tables for the bivariate and univariate distributions, respectively. The resulting pgf equations for a steady-state CSTR are presented in **Table 4**. The relationship between the pgf balances for CSTR and for a semibatch reactor are the same as for the population balances.

In these equations, $\phi_{0,0}^b(z1, z2)$, $\phi_0^{lin}(z1)$, $\psi_{0,0}^{b=}(z1, z2)$, $\psi_0^{lin=}(z1)$, $\psi_{0,0}^b(z1, z2)$ and $\psi_0^{lin}(z1)$ are the pgfs of the distributions of $R_{n,i}^b$, $R_{n,1}^{lin}$, $P_{n,i}^{b=}$, $P_{n,1}^{lin=}$, $P_{n,i}^b$ and $P_{n,1}^{lin}$, respectively.

The bivariate distributions of the branched chains and the univariate distributions of the linear chains are connected in the distribution of the total concentration of dead polymer chains with a terminal double bond, $P_{n,i}^-$. The total concentration of dead polymer chains with a terminal double bond is part of the mass balance of the growing polymer radicals in a CGC-Ti catalyst shown in Eq.(42). As mentioned above, $P_n^- = P_{n,i}^{b=} + P_{n,i}^{lin=}$ and $P_{n,i}^{lin=} = 0$ for $i=2, \dots, \infty$. Taking this into account, applying the bivariate pgf definition (Eq. (1)) we obtain:

$$\psi_{0,0}^-(z1, z2) = \psi_{0,0}^{b=}(z1, z2) + z2\psi_0^{lin=}(z1) \quad (54)$$

This expression can be applied in the pgf balance of $\phi_{0,0}^b(z1, z2)$ (Eq. (48)). Finally, the pgf of the total population of dead polymer species $P_{n,i} = P_{n,i}^{b=} + P_{n,i}^{lin=} + P_{n,i}^b + P_{n,i}^{lin}$ is

$$\psi_{0,0}(z1, z2) = \frac{\mu_{0,0}^{b=}\psi_{0,0}^{b=}(z1, z2) + \mu_{0,0}^b\psi_{0,0}^b(z1, z2) + z2\mu_0^{lin=}\psi_0^{lin=}(z1) + z2\mu_0^{lin}\psi_0^{lin}(z1)}{\mu_{0,0}^{b=} + \mu_{0,0}^b + \mu_0^{lin=} + \mu_0^{lin}} \quad (55)$$

Zero order moments of the polymer species distributions are involved in the pgf balance equations. Therefore, the balance equations for these moments and for the pgfs must be solved simultaneously. The moment equations are drawn from the balance equations of the polymeric species (Eqs. (42)-(47)) using well-known techniques. The moment balances for a steady-state CSTR are shown in Table 5.

The complete set of model equations includes the pgf balances (Eqs. (48)-(53)), Eq. (54) and (55), the moment balances (Eqs. (56)-(61)), the balances of the activated catalysts (Eqs. (40) and (41)) and the pgf inversion method equations (Eq. (33)). The bivariate MWD-LCBD of the total population of dead polymer chains will be reported below. Since the chain length domain has an order of magnitude of 10^5 , the 2D PAP-IFG method was used. The Papoulis part of the inversion method is applied to the chain length domain, while the IFG part is applied to the branch domain (order of magnitude 10). The pgf balances have to be solved for all pairs of (z_1, z_2) values required by the inversion method. It should be noted that bivariate pgfs are complex variables. Therefore, the pgf equations in which they are involved were split into separate equations for their real and complex components in the solution procedure. Additional process conditions needed to solve the model equations are shown in **Table 6**.

Figure 5 shows the bivariate MWD-LCBD predicted by the 2D PAP-IFG method. The distribution was also computed by direct solution of the original large system of population balances of the polymeric species (Eqs. (42)-(47)) in order to assess the goodness of the pgf technique. The pgf solution was very accurate. Parameters N_P and N_2 were both set to 10, according to the guidelines presented above. The value of N_2 is larger than the maximum significant value in the dimension of the number of branches, which ensures a negligible error in the inversion in this dimension. At the same time, a good convergence in the selection of the value of parameter N_P was observed. This resulted in the accurate prediction of the bivariate MWD-LCBD presented in Fig 5.

Even though in some systems the Papoulis part of the 2D PAP-IFG inversion method could be unsatisfactory, the thorough tests we have performed suggest that a good performance should be expected for most systems. In those cases in which the 2D PAP-IFG method does not exhibit a good performance, the 2D IFG method would provide an error-free inversion, possibly at the expense of longer computational times.

The computed MWD-LCBD shows that the polymer sample is characterized by a large proportion of linear chains with respect to branched chains. It can also be observed that, as expected, chains with higher branch content have higher molecular weights. It is important to note the difference in two orders of magnitude in the bivariate distribution between linear ($m = 1$) and branched chains ($m \geq 2$), which was also obtained by the pgf solution with high precision.

The number of pgf equations for this model is $n_{\text{eq}} = 6 \cdot 2 \cdot n_{\text{ev}} = 12N_n (N_p + 1) \left(\frac{N_2}{2} + 1 \right) = 12 \cdot 31 \cdot (10 + 1) \left(\frac{10}{2} + 1 \right) = 24552$. This number takes into account that there are six different pgf variables corresponding to the six polymeric species, and that each of these pgf evaluations requires two equations, one for the real and one for the imaginary component of the pgf. On the other hand, solving the original set of population balances is useful for comparing the pgf results, but it is extremely demanding. Since the population balances need to be parameterized for all chains from 1 to the maximum significant chain length, the total number of equations is $6 \cdot 100000 = 600000$.

The two inversion methods presented in this work (the 2D IFG and the 2D PAP-IFG methods) rely on the availability of accurate values for the 2D pgfs, which are obtained from the solution of the (usually stiff) system of the model equations. Standard DAE solvers with error control can be used for solving the mathematical model of the process.

Figure 6 shows the time evolution of the bivariate MWD-LCBD in a semibatch reactor. At initial time, the chain population consists mostly of linear chains. As time progresses, the concentration of linear chains slightly decreases as those with terminal double bond react to form branched molecules. Chains with higher branch content are formed as the reaction proceeds. As expected, chains with a larger number of branches have higher molecular weights. It can be noted that each population of branched chains (i.e. with a given number of branches) increases in concentration as the reaction proceeds over the time interval, and that the peaks of these individual distributions tend to move to lower molecular weights.

Figure 7 shows the effect of the concentration of H₂ on the bivariate MWD-LCBD. Hydrogen is used in the operation of this process to control the molecular weight, but it affects the branching distribution as well. It can be observed that when the concentration of H₂ is increased, the molecular weight of the polymer decreases (curves shift to lower chain lengths). The effect on the branching distribution depends on the branch content of the chains. The height of the curves indicates that the concentration of chains with lower branch content ($m \leq 3$) increases when the concentration of H₂ is increased. The opposite effect is observed for chains with higher branch content. Note that curve areas should have been compared, but in this case their height follows the same trend and they are easier to read in the graph.

Figure 8 illustrates the influence of the ratio of the constrained geometry catalyst in the catalyst mix on the bivariate MWD-LCBD. Linear chains and those with up to one branch ($m = 2$) are included in the figure. The behavior of chains with higher branch content is similar to the latter. The constrained geometry catalyst is the one that allows incorporating branches on growing polymer chains by means of the propagation of terminal double bonds. When its ratio is increased, the concentration of linear chains decreases. At the same time, the molecular weight of branched chains increases. Besides, their concentration reaches a maximum for a particular value of r_{CGC} . For chains with up to two branches ($m = 3$), this maximum is observed at

$r_{CGC} = 0.8$, as shown in the figure for the case of $m = 2$. For chains with more branches, the maximum is observed at $r_{CGC} = 0.4$.

As for the semibatch model, it is not possible to provide a comparison with the direct integration of the mass balances of Eqs. (42)-(47). An implicit method is needed due to the stiffness of the system of equations. The size of this system is large (600000 equations as mentioned above), and the implicit method requires a Jacobian matrix with a corresponding squared dimension. This leads to a prohibitively large memory allocation space. The solution of the mass balances for the CSTR reactor could be achieved because, in that case, the 600000 algebraic equations can be solved recursively for increasing values of n , since the mass balances of species of chain length n only depend on species of shorter lengths. For the semibatch model with the pgf equations, parameters N_P and N_2 were set to $N_P = 6$ and $N_2 = 10$ solving for $N_n = 31$ points, so

$$\begin{aligned} \text{the number of equations was } n_{\text{eq}} &= 6 \cdot 2 \cdot n_{\text{ev}} = 12N_n (N_P + 1) \left(\frac{N_2}{2} + 1 \right) \\ &= 12 \cdot 31 \cdot (6 + 1) \left(\frac{10}{2} + 1 \right) = 15624. \end{aligned}$$

It is worth noting that the 2D pgf technique can be used for modeling bivariate distributions of polymer properties in any system whose elementary reaction steps are included in the 2D pgf Transform Table presented in our previous work (Brandolin & Asteasuain, 2013). This includes all the usual copolymer systems and branched polymers systems prior to the gel point. Only systems for which the termination rate constant is chain-length dependent cannot be modeled, because with the state-of-art 2D pgf technique it is not possible to obtain the pgf transform of chain-length dependent termination reactions. For the inversion step of the 2D pgf technique, both inversion methods presented in this work allow applying the pgf methodology to polymer systems without constraints on the range of values of the distributed properties.

4. Conclusions

In this work two inversion methods of 2D pgfs, which are a key component of the 2D pgf technique for modeling bivariate distributions of polymer properties, are presented. They were developed with a focus on recovering pgf transforms of bivariate distributions characterized by independent domains with different ranges of values. The first method is based on a double application of an inversion method of complex univariate pgfs. The second method combines the univariate inversion method of complex pgfs with a univariate inversion method of real pgfs. Both 2D inversion methods exhibited very good accuracy. From the point of view of the number of pgf evaluations, the first method is more appropriate when the ranges of values of the independent domains of the bivariate distribution are not too large. On the other hand, the second method becomes advantageous when the range of values of the larger independent domain increases. The complete 2D pgf technique was successfully applied to the prediction of the bivariate MWD-LCBD of a polyethylene produced by a mixed metallocene system, showing the potential of this method for modeling bivariate distributions of polymer properties of any type. Finally, this methodology has potential as a tool in industrial polymer processes to aid the synthesis of polymers with prespecified molecular architecture.

Acknowledgements: the authors wish to thank The Nacional Research Council of Argentina (CONICET), the National Agency of Scientific and Technological Promotion (ANPCyT) and Universidad Nacional del Sur (UNS) for financial support.

References

Abate J, Choudhury GL, Whitt W. Numerical Inversion of Multidimensional Laplace Transforms by the Laguerre Method. *Perform Evaluation* 1998; 31: 229-43.

- Abate J, Choudhury GL, Whitt W. (2000). An Introduction to Numerical Transform Inversion and its Application to Probabilty Models. In W. K. Grassmann (Ed.), Computational Probability. New York: Springer Science+Business Media, LLC.
- Abate J, Whitt W. Numerical inversion of probability generating functions. Oper Res Lett 1992; 12: 245-51.
- Abiko Y, Nakabayashi K, Mori H. RAFT Polymerization of Phenyl Vinyl Sulfide Using Trithiocarbonate Mediating Agents and Synthesis of Block Copolymers. Macromol Symp 2015; 349: 34-43.
- Ali Parsa M, Kozhan I, Wulkow M, Hutchinson RA. Modeling of Functional Group Distribution in Copolymerization: A Comparison of Deterministic and Stochastic Approaches. Macromol Theory Simul 2014; 23: 207-17.
- Asteasuain M. (2003). Modelado de Procesos de Polimerización y Procesos Pos Reactor. Aplicación de Nuevas Técnicas para la Predicción de la Distribución de Pesos Moleculares con Verificación Experimental. Unpublished Ph.D., Universidad Nacional del Sur, Bahía Blanca, Argentina.
- Asteasuain M, Brandolin A. Mathematical Modeling of Bivariate Polymer Property Distributions Using 2D Probability Generating Functions, 1 - Numerical Inversion Methods. Macromol Theory Simul 2010; 19: 342-59.
- Asteasuain M, Sarmoria C, Brandolin A. Recovery of Molecular Weight Distributions from Transformed Domains. Part I: Application of pgf to Mass Balances Describing Reactions Involving Free Radicals. Polymer 2002; 43: 2513-27.
- Brancik L. (2002). Improved method of numerical inversion of two-dimensional Laplace transforms for dynamical systems simulation. In Electronics, Circuits and Systems, 2002 9th International Conference on (Vol. 1, pp. 385-8 vol.1).
- Brančík L. (2010). Technique of 3D NILT based on complex Fourier series and quotient-difference algorithm. In (pp. 203-6). Athens.

- Brandolin A, Asteasuain M. Mathematical Modeling of Bivariate Distributions of Polymer Properties Using 2D Probability Generating Functions. Part II: Transformation of Population Mass Balances of Polymer Processes. *Macromol Theory Simul* 2013; 22: 273-308.
- Butté A, Storti G, Morbidelli M. Evaluation of the Chain Length Distribution in Free-Radical Polymerization, 1. Bulk Polymerization. *Macromol Theory Simul* 2002; 11: 22-36.
- Cavers JK. On the Fast Fourier Transform Inversion of Probability Generating Functions. *J I Math Appl* 1978; 22: 275-82.
- Costeux S. Statistical Modeling of Randomly Branched Polymers Produced by Combination of Several Single-Site Catalysts: Toward Optimization of Melt Properties. *Macromolecules* 2003; 36: 4168-87.
- Chao Z, Shao-hai H, Yang X, Xue-fen W. (2008). The application of 2-D numerical inversion of Laplace transform. In *Signal Processing, 2008 ICSP 2008 9th International Conference on* (pp. 60-3).
- Chen J, Zhao X, Zhang L, Cheng Z, Zhu X. Reversible addition-fragmentation chain transfer polymerization of vinyl acetate under high pressure. *J Polym Sci Polymer Chem* 2015; 53: 1430-6.
- Daigle JN. Queue Length Distributions from Probability Generating Functions via Discrete Fourier Transforms. *Oper Res Lett* 1989; 8: 229-36.
- Dow Polyethylene, 2011,
http://www.dow.com/polyethylene/global_news/2011/20110404a.htm. (accessed 27.06.2016).
- Fortunatti C, Sarmoria C, Brandolin A, Asteasuain M. Modeling of RAFT Polymerization using Probability Generating Functions. Detailed Prediction of Full Molecular Weight Distributions and Sensitivity Analysis. *Macromol React Eng* 2014; 8: 781-95.

- Gianoglio Pantano IA, Asteasuain M, Díaz MF, Sarmoria C, Brandolin A. Catalytic Degradation of Polystyrene: Modeling of Molecular Weight Distribution. *Macromol React Eng* 2011; 5: 243-53.
- Gianoglio Pantano IA, Asteasuain M, Sarmoria C, Brandolin A. Graft Copolymers for Blend Compatibilization: Mathematical Modeling of the Grafting Process. *Macromol React Eng* 2012; 6: 406-18.
- Iedema PD, Hoefsloot HCJ. Predicting Molecular Weight and Degree of Branching Distribution of Polyethylene for Mixed Systems with a Constrained Geometry Metallocene Catalyst in Semibatch and Continuous Reactors. *Macromolecules* 2003; 36: 6632-44.
- Iedema PD, Wulkow M, Hoefsloot HCJ. Modeling Molecular Weight and Degree of Branching Distribution of Low-Density Polyethylene. *Macromolecules* 2000; 33: 7173-84.
- Kizilel S, Papavasiliou G, Gossage J, Teymour F. Mathematical Model for Vinyl-Divinyl Polymerization. *Macromol React Eng* 2007; 1: 587-603.
- Krallis A, Meimaroglou D, Kiparissides C. Dynamic prediction of the bivariate molecular weight-copolymer composition distribution using sectional-grid and stochastic numerical methods. *Chem Eng Sci* 2008; 63: 4342-60.
- Kryven I, Iedema PD. A Novel Approach to Population Balance Modeling of Reactive Polymer Modification Leading to Branching. *Macromol Theory Simul* 2013; 22: 89-106.
- Lazzari S, Storti G. Modeling Multiradicals in Crosslinking MMA/EGDMA Bulk Copolymerization. *Macromol Theory Simul* 2014; 23: 15-35.
- Meimaroglou D, Krallis A, Saliakas V, Kiparissides C. Prediction of the bivariate molecular weight - Long chain branching distribution in highly branched polymerization systems using Monte Carlo and sectional grid methods. *Macromolecules* 2007; 40: 2224-34.

- Mills P, L. Determination of polymer chain length distributions by numerical inversion of z-transforms. *Computers and Chemical Engineering* 1986; 10: 399-420.
- Papavasiliou G, Teymour F. Reconstruction of the chain length distribution for vinyl-divinyl copolymerization using the numerical fractionation technique. *Macromol Theory Simul* 2003; 12: 543-8.
- Pladis P, Meimaroglou D, Kiparissides, C. Prediction of the Viscoelastic Behavior of Low-Density Polyethylene Produced in High-Pressure Tubular Reactors. *Macromol React Eng* 2015; 9: 271-84.
- Pladis P, Kiparissides C. A comprehensive model for the calculation of molecular weight-long-chain branching distribution in free-radical polymerizations. *Chem Eng Sci* 1998; 53: 3315-33.
- Schütte C, Wulkow M. A Hybrid Galerkin–Monte-Carlo Approach to Higher-Dimensional Population Balances in Polymerization Kinetics. *Macromol React Eng* 2010; 4: 562-77.
- Singh M, Chakraborty J, Kumar J, Ramakanth R. Accurate and efficient solution of bivariate population balance equations using unstructured grids. *Chem Eng Sci* 2013; 93: 1-10.
- Singhal K, Vlach J, Vlach M. Numerical inversion of multidimensional Laplace transform. *Proceedings of the IEEE* 1975; 63: 1627-8.
- Soares JBP, Hamielec AE. The chemical composition component of the distribution of chain length and long chain branching for copolymerization of olefins and polyolefin chains containing terminal double-bonds. *Macromol Theory Simul* 1997; 6: 591-6.
- Valkó PP, Abate J. Numerical inversion of 2-D Laplace transforms applied to fractional diffusion equations. *Appl Numer Math* 2005; 53: 73-88.
- Wulkow M. Computer Aided Modeling of Polymer Reaction Engineering—The Status of Prediction, 1 - Simulation. *Macromol React Eng* 2008; 2: 461-94.
- Xiao Y, Lee MH. 2-D Laplace-Z Transformation. *IEICE TRANS Fundamentals* 2006; E89-A: 1500-4.

Zapata-González I, Saldívar-Guerra E, Ortiz-Cisneros J. Full Molecular Weight Distribution in RAFT Polymerization. New Mechanistic Insight by Direct Integration of the Equations. *Macromol Theory Simul* 2011; 20: 370-88.

Appendix

A.1. Error of the 2D IFG inversion method: sensitivity to the values of parameters N_1 and N_2

To simplify the analysis, N_1 was kept at the value of 140 used in the examples shown in the main text, while N_2 was set to 12, 10 and 8. The results are shown in **Figs A. 1-A. 3**. Note that as N_1 is kept in a conservative value, only the error in the direction of m is affecting the results.

That is, the error expression in Eq. (25) reduces to $e(n, m) = \sum_{k=1}^{\infty} p(n, m + kN_2)$.

The error increases as N_2 becomes smaller, as predicted by Eq. (25), because a larger portion of the true distribution is “left out”, affecting the computed distribution as explained in the main text. The distribution points for the lower values of m are the most affected, since the larger values of the descending “left out” portion of distribution are summed to them. **Table A. 1** shows an example of the accuracy of the error formula shown in Eq. (25). Minor differences between the actual and theoretical errors arise from round off error in the numerical evaluation of the inversion formula presented in Eq. (22). Results similar to the ones shown in **Figs A. 1-A. 3** and in **Table A. 1** are obtained when changing the values of N_1 instead of N_2 , and for distribution $p^2(n, m)$.

A.2. Error of the 2D IFG-PAP inversion method: sensitivity to the values of parameter N_p

The procedure for selecting the value of N_p for the 2D IFG-PAP method is illustrated in **Fig A. 4** for distribution $p^1(n, m)$. The whole distribution was recovered, but for the sake of clarity

only the results corresponding to $m = 5$ are shown. The recovered distributions tend to converge as N_p increases from 23 to 35. In fact, distributions computed using N_p from 30-35 almost coincide. Slight differences begin to appear at $N_p = 37$, while the round-off error causes a completely wrong distribution at $N_p = 41$. Finally, $N_p = 30$ was selected from the set of coincident distributions. The analytical distribution is included in the figure to show that the recovered distributions converge to the true distribution, but it is not required in the process of assigning parameter N_p . The accuracy in the inversion, that is, the distance between the converged distribution and the true distribution, cannot be guaranteed. In general, accuracy cannot be assured for methods based on Laplace transform inversion. However, experience shows that the higher the confidence in the convergence procedure (i.e. the higher the number of very similar distributions in the convergence zone), the higher is the accuracy in the inversion.

Similar results were obtained for distribution $p^2(n, m)$. It should be mentioned that once an appropriate value of N_p is selected, this value works well for distributions resulting from similar conditions (i.e. similar values of μ_1 and μ_2 for distribution $p^1(n, m)$, similar process conditions for a MWD in a polymerization process). Therefore, it is not necessary to re-set N_p each time a new distribution is computed.

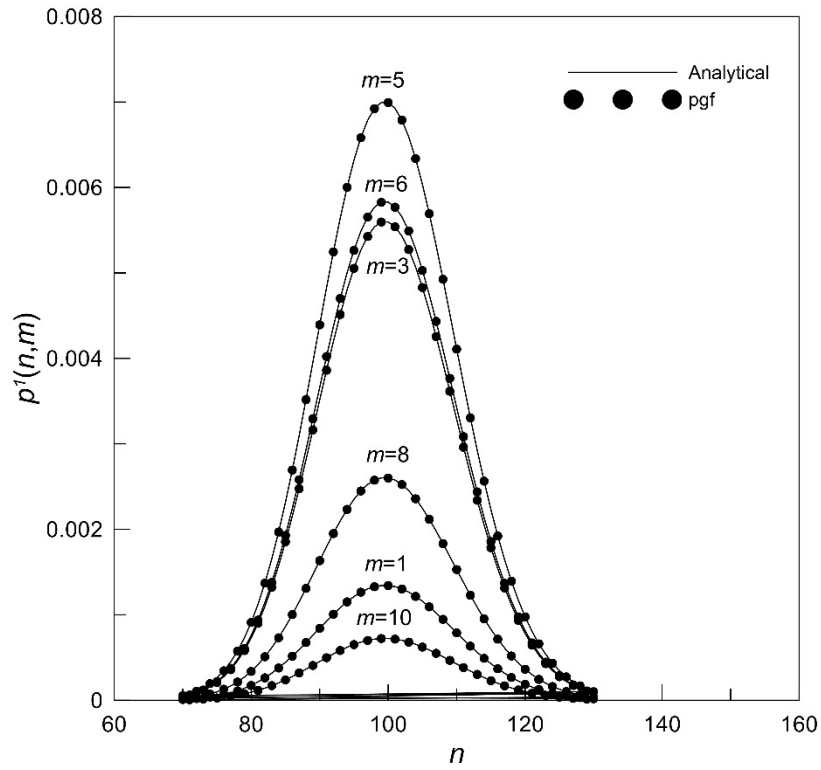


Fig 1. Analytical distribution $p^1(n, m)$ recovered with the 2D IFG method.

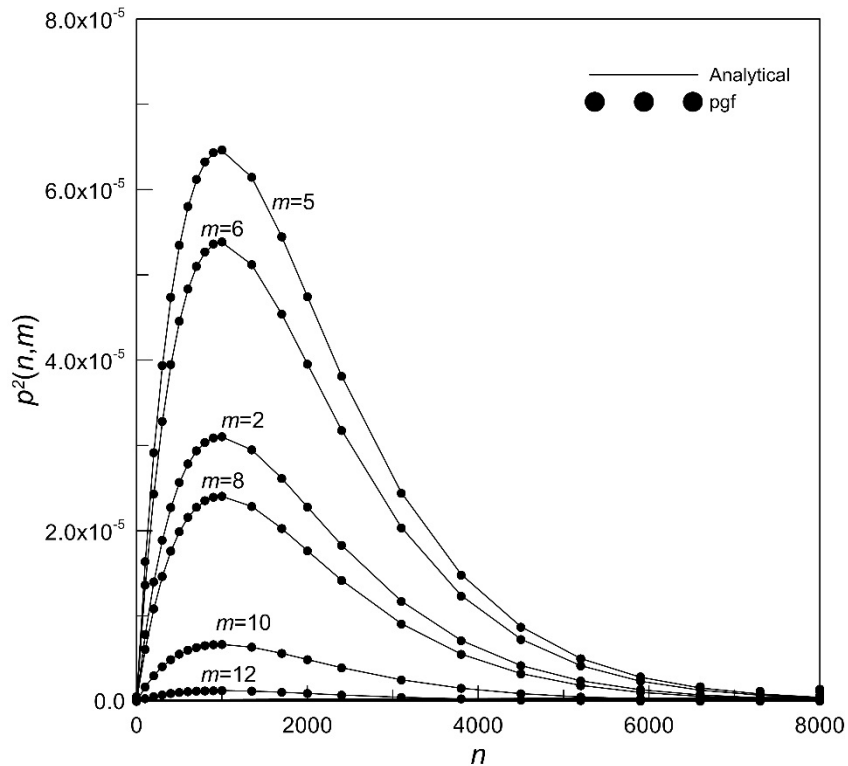


Fig 2. Analytical distribution $p^2(n, m)$ recovered with the 2D IFG method.

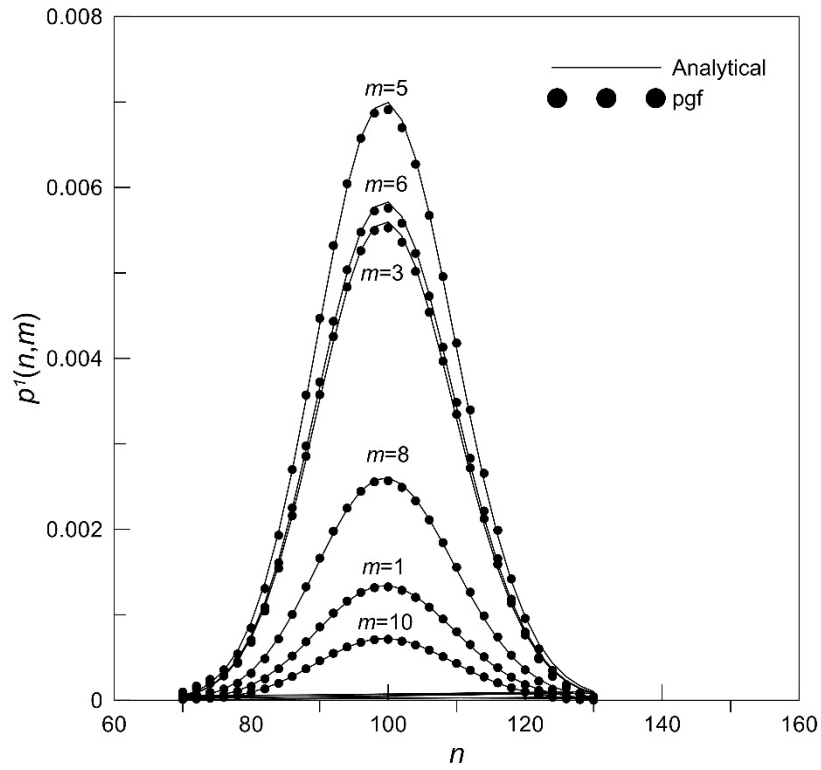


Fig 3. Analytical distribution $p^1(n, m)$ recovered with the 2D PAP-IFG method.

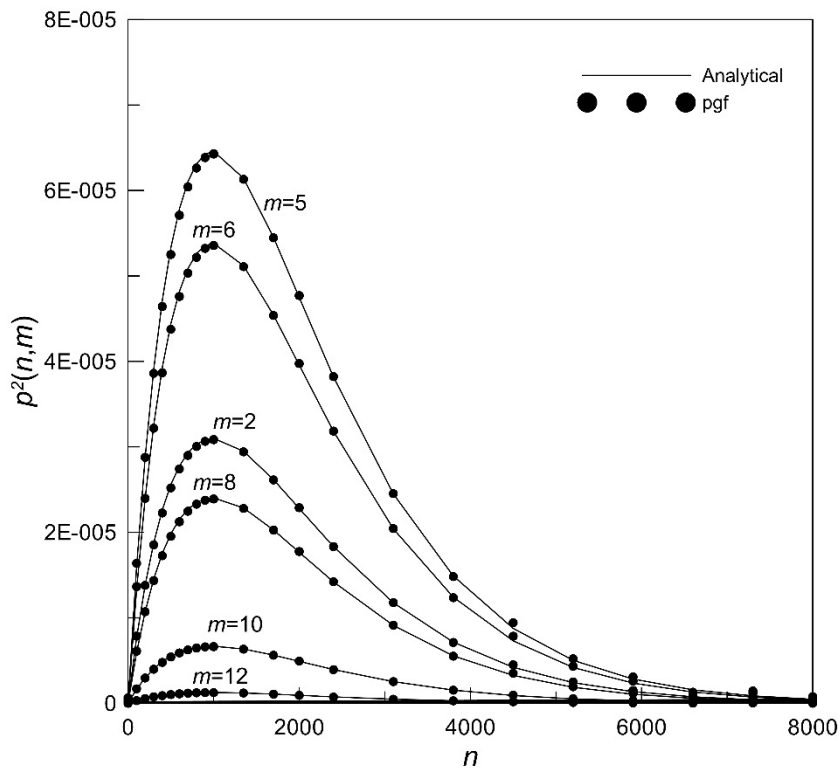


Fig 4. Analytical distribution $p^2(n, m)$ recovered with the 2D PAP-IFG method.

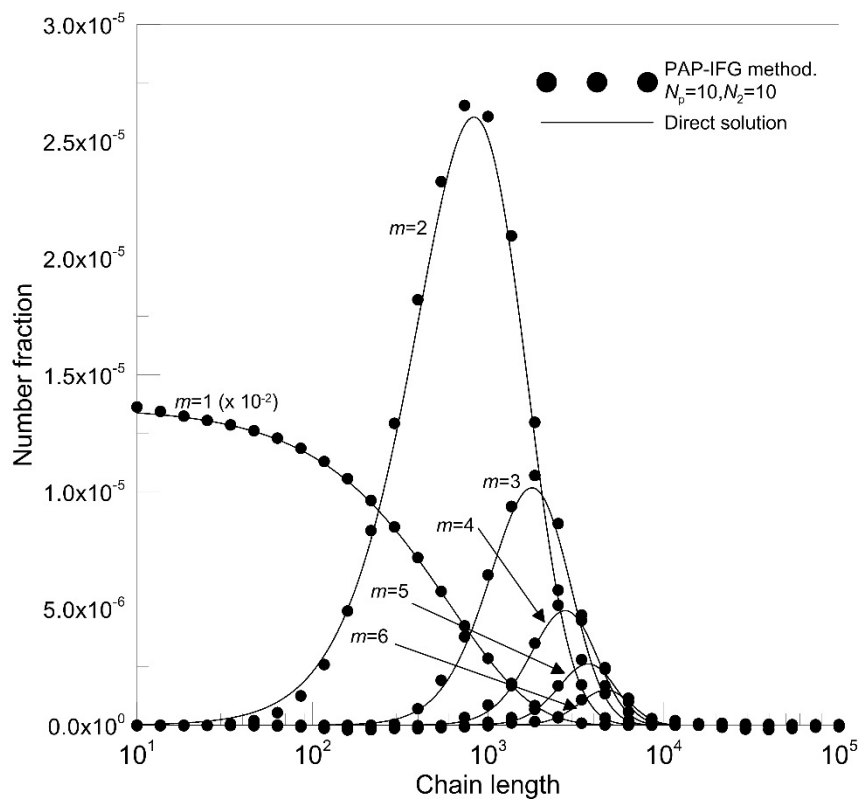


Fig 5. Bivariate MWD-LCBD of the polyethylene produced in the mixed catalyst system in a steady-state CSTR reactor.

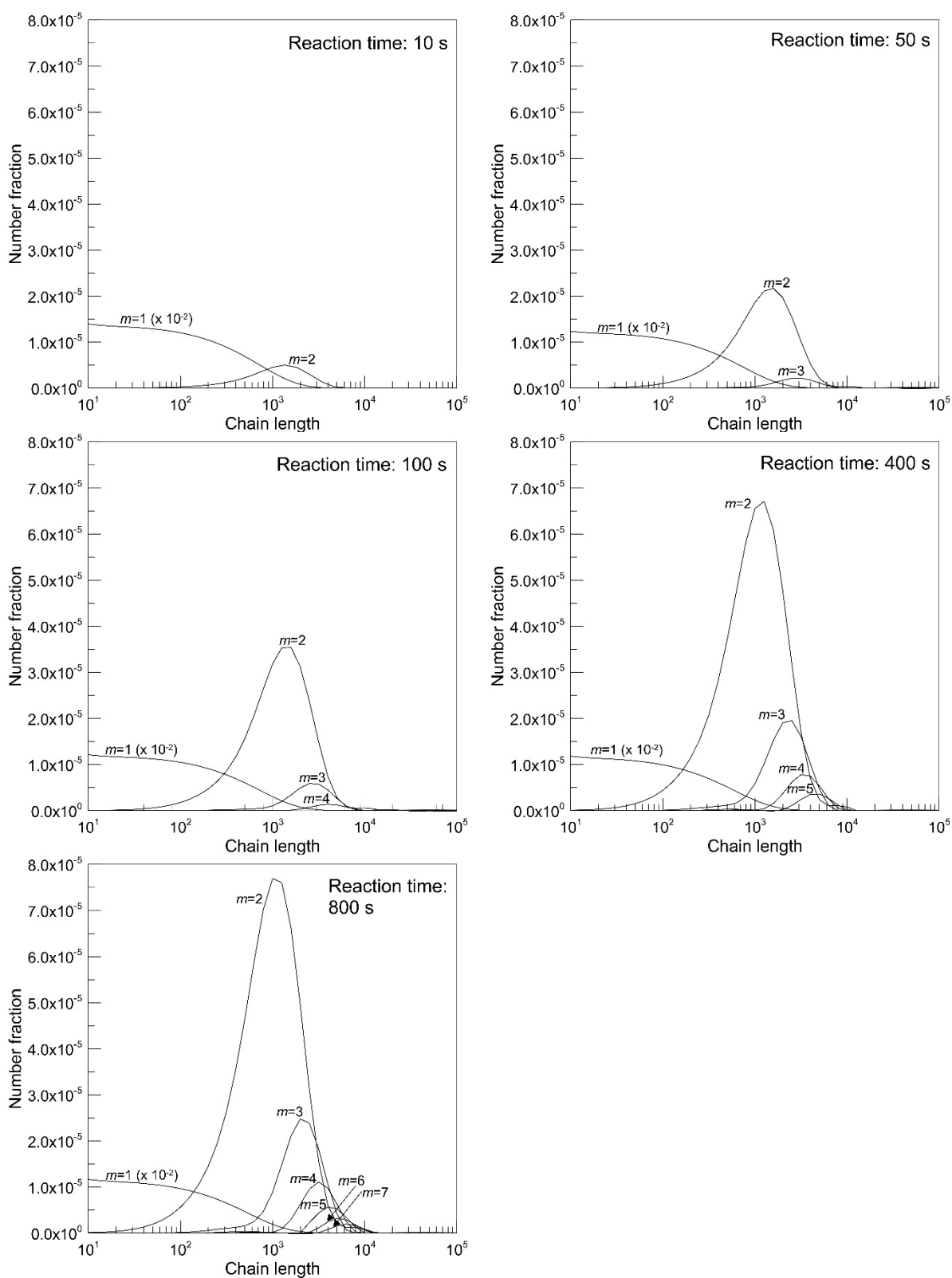


Fig 6. Time evolution of the bivariate MWD-LCBD of the polyethylene produced in the mixed catalyst system in a semibatch reactor. Parameters of the pgf method: $N_P = 6$, $N_2 = 10$.

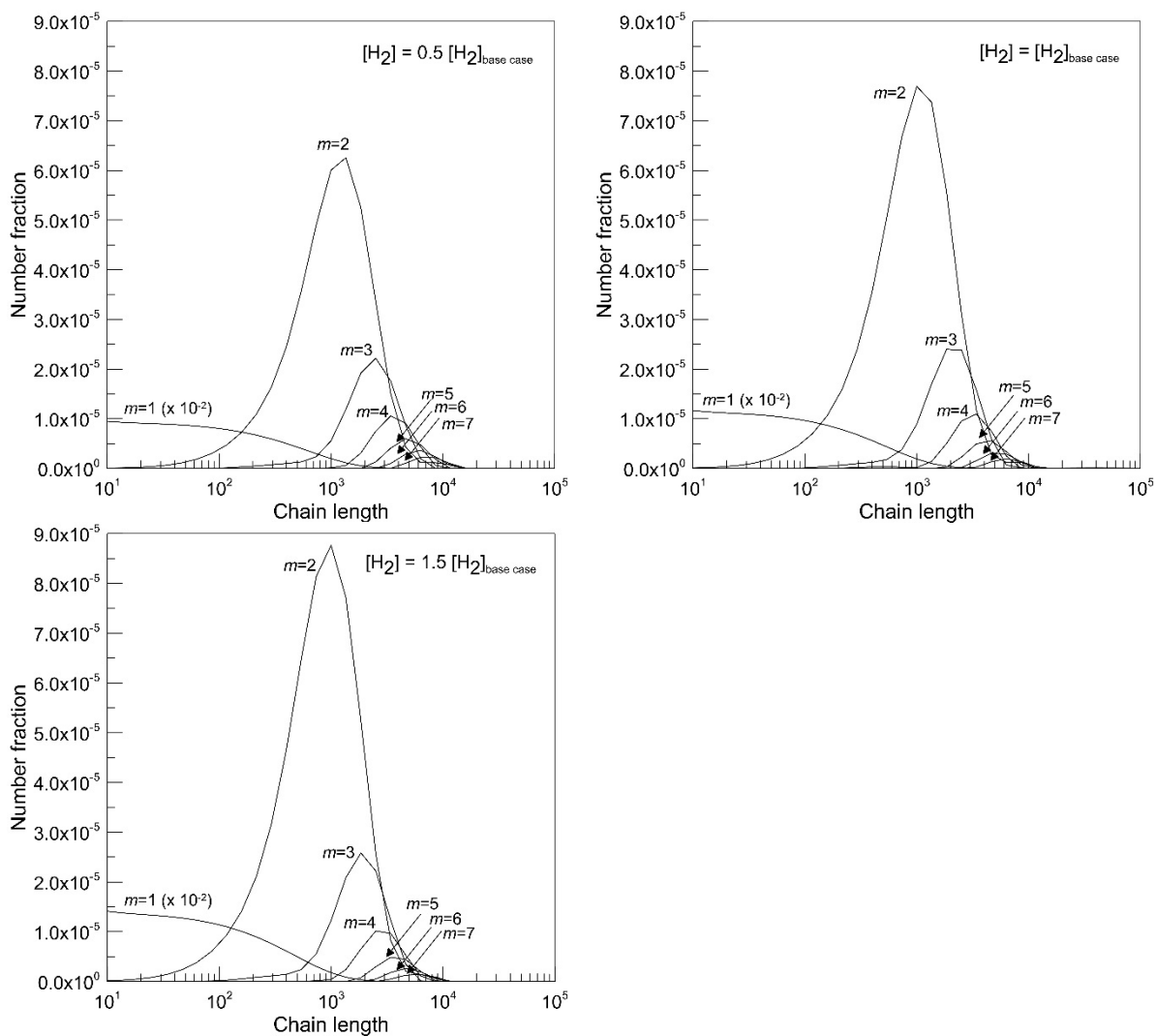


Fig 7. Effect of the concentration of H_2 on the bivariate MWD-LCBD of the polyethylene produced in the mixed catalyst system in a semibatch reactor. $[H_2]_{\text{base case}}$ is the concentration of H_2 reported in Table 6; reaction time: 800 s. Parameters of the pgf method: $N_P = 6$, $N_2 = 10$.

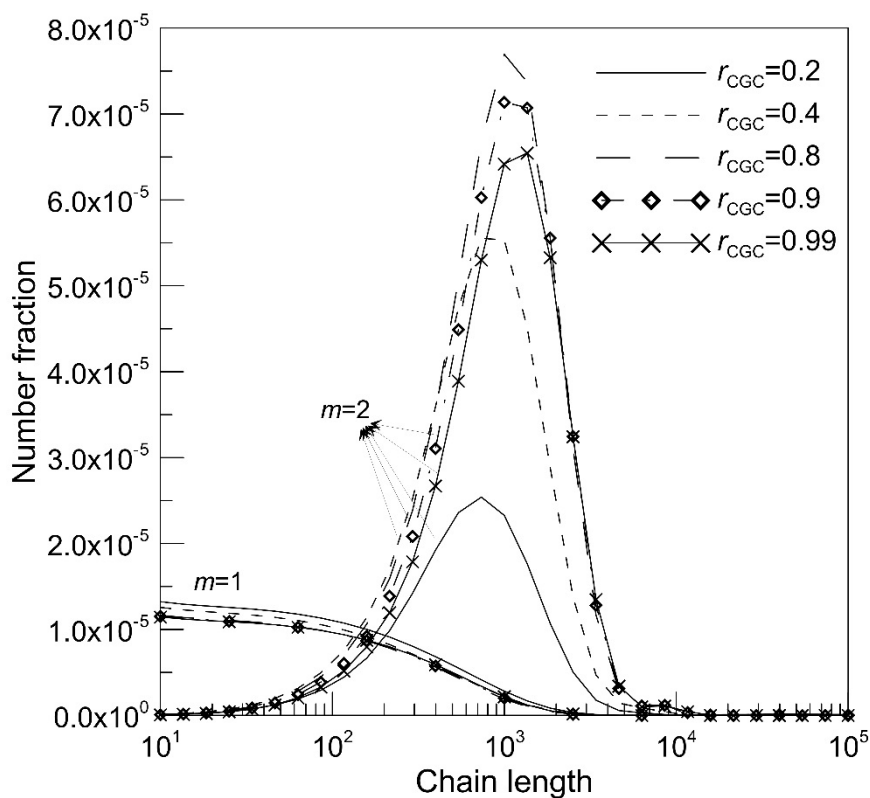


Fig 8. Effect of the ratio of constrained geometry catalyst in the catalyst mix (r_{CGC}) on the bivariate MWD-LCBD of the polyethylene produced in the mixed catalyst system in a semibatch reactor. Reaction time: 800 s. Parameters of the pgf method: $N_p = 6$, $N_2 = 10$.

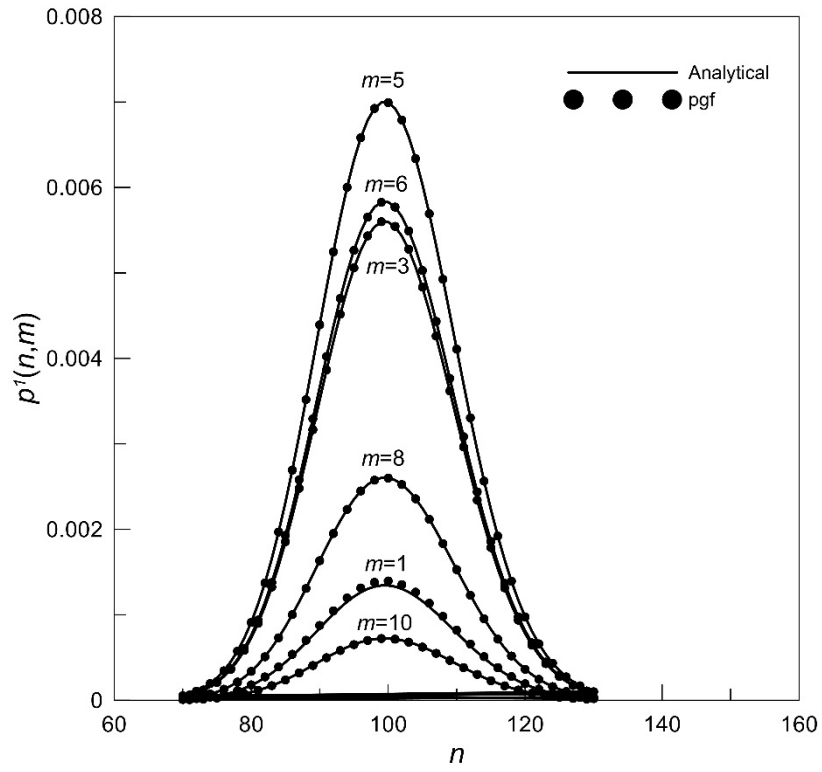


Fig A. 1. Analytical distribution $p^1(n, m)$ recovered with the 2D IFG method with $N_1 = 140$ and $N_2 = 12$ (error slightly affects the curve of $m = 1$, see Fig 1 for comparison).

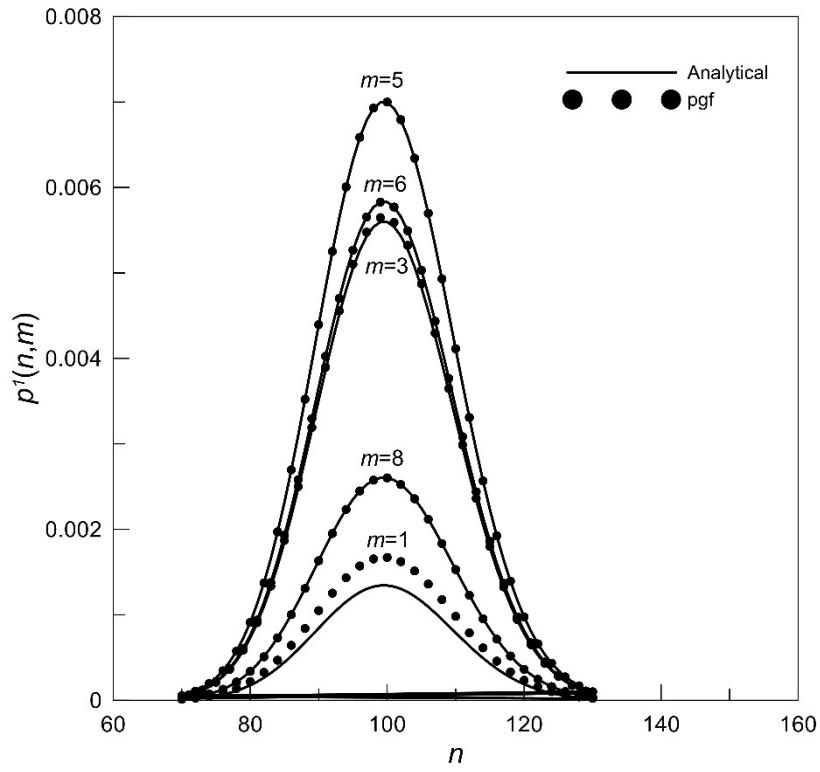


Fig A. 2. Analytical distribution $p^1(n, m)$ recovered with the 2D IFG method with $N_1 = 140$ and $N_2 = 10$ (the curve corresponding to $m = 10$ was not included since $m \leq N_2 - 1$).

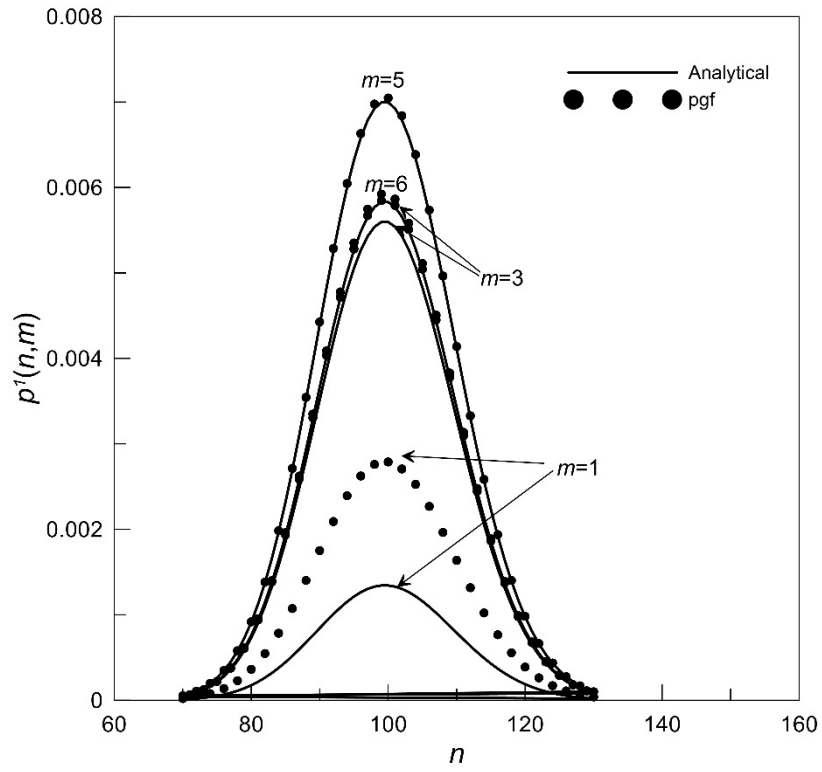


Fig A. 3. Analytical distribution $p^1(n, m)$ recovered with the 2D IFG method with $N_1 = 140$ and $N_2 = 8$ (the curve corresponding to $m = 8$ was not included since $m \leq N_2 - 1$).

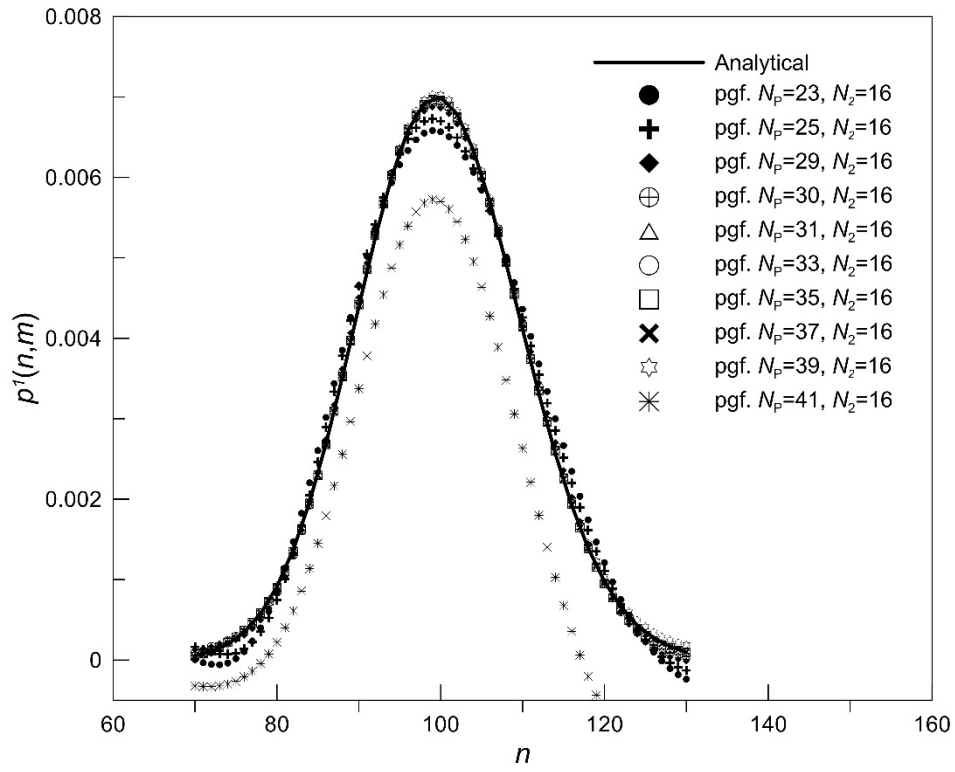


Fig A. 4. Analytical distribution $p^1(n, m)$, $m = 5$, recovered with the 2D PAP-IFG method with $N_p = 23-41$ and $N_2 = 16$.

Table 1. Kinetic mechanism for the polymerization of ethylene using a mixed metallocene catalyst system.

Step	Kinetic equation
CGC-Ti activation and initiation	$C_{CGC} \xrightarrow{k_{a,CGC}} C_{CGC}^*$
	$C_{CGC}^* + M \xrightarrow{k_{i,CGC}} R_{1,1}^b$
Et[Ind] ₂ ZrCl ₂ activation and initiation	$C_{lin} \xrightarrow{k_{a,lin}} C_{lin}^*$
	$C_{lin}^* + M \xrightarrow{k_{i,lin}} R_{1,1}^{lin}$
Propagation CGC-Ti	$R_{n,i}^b + M \xrightarrow{k_{p,CGC}} R_{n+1,i}^b$
Propagation Et[Ind] ₂ ZrCl ₂	$R_{n,1}^{lin} + M \xrightarrow{k_{p,lin}} R_{n+1,1}^{lin}$
β -hydride elimination CGC-Ti	$R_{n,i}^b \xrightarrow{k_{\beta,CGC}} C_{CGC}^* + P_{n,i}^{b=}$
β -hydride elimination Et[Ind] ₂ ZrCl ₂	$R_{n,1}^{lin} \xrightarrow{k_{\beta,lin}} C_{lin}^* + P_{n,1}^{lin=}$
Transfer to monomer CGC-Ti	$R_{n,i}^b + M \xrightarrow{k_{M,CGC}} C_{CGC}^* + P_{n,i}^{b=}$
Transfer to monomer Et[Ind] ₂ ZrCl ₂	$R_{n,1}^{lin} + M \xrightarrow{k_{M,lin}} C_{lin}^* + P_{n,1}^{lin=}$
Transfer to hydrogen CGC-Ti	$R_{n,i}^b + H_2 \xrightarrow{k_{H,CGC}} C_{CGC}^* + P_{n,i}^b$
Transfer to hydrogen Et[Ind] ₂ ZrCl ₂	$R_{n,1}^{lin} + H_2 \xrightarrow{k_{H,lin}} C_{lin}^* + P_{n,1}^{lin}$
Terminal double bond propagation CGC-Ti	$R_{n,i}^b + P_{m,j}^= \xrightarrow{k_{p,TDP}} R_{n+m,i+j}^b$
Catalyst deactivation (growing chains) CGC-Ti	$R_{n,i}^b \xrightarrow{k_{d1,CGC}} C_{CGC}^i + P_{n,i}^{b=}$
Catalyst deactivation (growing chains) Et[Ind] ₂ ZrCl ₂	$R_{n,1}^{lin} \xrightarrow{k_{d1,lin}} C_{lin}^i + P_{n,1}^{lin=}$
Catalyst deactivation (active catalyst) CGC-Ti	$C_{CGC} \xrightarrow{k_{d2,CGC}} C_{CGC}^i$
Catalyst deactivation (active catalyst) Et[Ind] ₂ ZrCl ₂	$C_{lin} \xrightarrow{k_{d2,lin}} C_{lin}^i$

Table 2. Kinetic parameters for the polymerization of ethylene using a mixed metallocene catalyst system (Iedema & Hoefsloot, 2003).

Kinetic constant	Value	Units
$k_{i,CGC}/k_{p,CGC}$	1	-
$k_{i,lin}/k_{p,lin}$	1	-
$k_{p,CGC} [M]$	500	s^{-1}
$k_{p,lin} [M]$	500	s^{-1}
$k_{\beta,CGC}$	0.3	s^{-1}
$k_{\beta,lin}$	0.7	s^{-1}
$k_{M,CGC}/k_{p,CGC}$	0	-
$k_{M,lin}/k_{p,lin}$	0	-
$k_{H,CGC}$	250	$m^3 \cdot kmol^{-1} \cdot s^{-1}$
$k_{H,lin}$	0	$m^3 \cdot kmol^{-1} \cdot s^{-1}$
$k_{P,TDP}$	1750	$m^3 \cdot kmol^{-1} \cdot s^{-1}$
$k_{d1,CGC} = k_{d2,CGC} = k_{d1,lin} = k_{d2,CGC}$	0	s^{-1}

Table 3. Population balance equations for a steady-state CSTR.

Species	Balance Equation
C_{CGC}^*	$0 = -k_{i,CGC} [M] C_{CGC}^* + (k_{\beta,CGC} + k_{M,CGC} [M] + k_{H,CGC} [H_2]) \sum_{n=1}^{\infty} \sum_{i=1}^{\infty} [R_{n,i}^b] - k_{d2,CGC} C_{CGC}^* + \frac{(C_{CGC,feed}^* - C_{CGC}^*)}{\tau}$ (40)
C_{lin}^*	$0 = -k_{i,lin} [M] C_{lin}^* + (k_{\beta,lin} + k_{M,lin} [M] + k_{H,lin} [H_2]) \sum_{n=1}^{\infty} [R_{n,1}^{lin}] - k_{d2,lin} C_{lin}^* + \frac{(C_{lin,feed}^* - C_{lin}^*)}{\tau}$ (41)
$R_{n,i}^b$	$0 = k_{i,CGC} [M] C_{CGC}^* \delta_{n,1} \delta_{i,1} + k_{p,CGC} [M] ([R_{n-1,i}^b] (1 - \delta_{n,1}) - [R_{n,i}^b]) - (k_{\beta,CGC} + k_{d1,CGC} + k_{M,CGC} [M] + k_{H,CGC} [H_2]) [R_{n,i}^b] + k_{p,TDP} \left(-[R_{n,i}^b] \sum_{m=1}^{\infty} \sum_{j=1}^{\infty} [P_{m,j}^=] + \sum_{m=1}^{n-1} \sum_{j=1}^{i-1} [P_{m,j}^=] [R_{n-m,i-j}^b] \right) + \frac{([R_{n,i,feed}^b] - [R_{n,i}^b])}{\tau}$ (42)
$R_{n,1}^{lin}$	$0 = k_{i,lin} [M] C_{lin}^* \delta_{n,1} + k_{p,lin} [M] ([R_{n-1,1}^{lin}] (1 - \delta_{n,1}) - [R_{n,1}^{lin}]) - (k_{\beta,lin} + k_{d1,lin} + k_{M,lin} [M] + k_{H,lin} [H_2]) [R_{n,1}^{lin}] + \frac{([R_{n,1,feed}^{lin}] - [R_{n,1}^{lin}])}{\tau}$ (43)
$P_{n,i}^{b=}$	$0 = (k_{\beta,CGC} + k_{d1,CGC} + k_{M,CGC} [M]) [R_{n,i}^b] - k_{p,TDP} [P_{n,i}^{b=}] \sum_{m=1}^{\infty} \sum_{j=1}^{\infty} [R_{m,j}^b] + \frac{([P_{n,i,feed}^{b=}] - [P_{n,i}^{b=}])}{\tau}$ (44)
$P_{n,1}^{lin=}$	$0 = (k_{\beta,lin} + k_{d1,lin} + k_{M,lin} [M]) [R_{n,1}^{lin}] - k_{p,TDP} [P_{n,1}^{lin=}] \sum_{m=1}^{\infty} \sum_{j=1}^{\infty} [R_{m,j}^b] + \frac{([P_{n,1,feed}^{lin=}] - [P_{n,1}^{lin=}])}{\tau}$ (45)
$P_{n,i}^b$	$0 = k_{H,CGC} [H_2] [R_{n,i}^b] + \frac{([P_{n,i,feed}^b] - [P_{n,i}^b])}{\tau}$ (46)
$P_{n,1}^{lin}$	$0 = k_{H,lin} [H_2] [R_{n,1}^{lin}] + \frac{([P_{n,1,feed}^{lin}] - [P_{n,1}^{lin}])}{\tau}$ (47)

Table 4. 2D pgf balance equations for a steady-state CSTR.

pgf	Balance Equation
$\phi_{0,0}^b(z1, z2)$	$0 = k_{i,CGC} [M] C_{CGC}^* z_1 z_2 + k_{p,CGC} [M] \left(z1 \left(\lambda_{0,0}^b \phi_{0,0}^b(z1, z2) \right) - \left(\lambda_{0,0}^b \phi_{0,0}^b(z1, z2) \right) \right) - \left(k_{\beta,CGC} + k_{d1,CGC} + k_{M,CGC} [M] + k_{H,CGC} [H_2] \right) \left(\lambda_{0,0}^b \phi_{0,0}^b(z1, z2) \right) + k_{p,TDP} \left(-\mu_{0,0}^- \left(\lambda_{0,0}^b \phi_{0,0}^b(z1, z2) \right) + \left(\lambda_{0,0}^b \phi_{0,0}^b(z1, z2) \right) \left(\mu_{0,0}^- \psi_{0,0}^- (z1, z2) \right) \right) + \frac{\left(\left(\lambda_{0,0}^b \phi_{0,0}^b(z1, z2) \right)_{\text{feed}} - \left(\lambda_{0,0}^b \phi_{0,0}^b(z1, z2) \right) \right)}{\tau}$ (48)
$\phi_0^{\text{lin}}(z1)$	$0 = k_{i,\text{lin}} [M] C_{\text{lin}}^* z1 + k_{p,\text{lin}} [M] \left(z1 \left(\lambda_0^{\text{lin}} \phi_0^{\text{lin}}(z1) \right) - \left(\lambda_0^{\text{lin}} \phi_0^{\text{lin}}(z1) \right) \right) - \left(k_{\beta,\text{lin}} + k_{d1,\text{lin}} + k_{M,\text{lin}} [M] + k_{H,\text{lin}} [H_2] \right) \left(\lambda_0^{\text{lin}} \phi_0^{\text{lin}}(z1) \right) + \frac{\left(\left(\lambda_0^{\text{lin}} \phi_0^{\text{lin}}(z1) \right)_{\text{feed}} - \left(\lambda_0^{\text{lin}} \phi_0^{\text{lin}}(z1) \right) \right)}{\tau}$ (49)
$\psi_{0,0}^{b=}(z1, z2)$	$0 = \left(k_{\beta,CGC} + k_{d1,CGC} + k_{M,CGC} [M] \right) \left(\lambda_{0,0}^b \phi_{0,0}^b(z1, z2) \right) - k_{p,TDP} \lambda_{0,0}^b \left(\mu_{0,0}^{b=} \psi_{0,0}^{b=}(z1, z2) \right) + \frac{\left(\left(\mu_{0,0}^{b=} \psi_{0,0}^{b=}(z1, z2) \right)_{\text{feed}} - \left(\mu_{0,0}^{b=} \psi_{0,0}^{b=}(z1, z2) \right) \right)}{\tau}$ (50)
$\psi_0^{\text{lin}=(z1)}$	$0 = \left(k_{\beta,\text{lin}} + k_{d1,\text{lin}} + k_{M,\text{lin}} [M] \right) \left(\lambda_0^{\text{lin}} \phi_0^{\text{lin}}(z1) \right) - k_{p,TDP} \lambda_{0,0}^b \left(\mu_0^{\text{lin}=} \psi_0^{\text{lin}=(z1)} \right) + \frac{\left(\left(\mu_0^{\text{lin}=} \psi_0^{\text{lin}=(z1)} \right)_{\text{feed}} - \left(\mu_0^{\text{lin}=} \psi_0^{\text{lin}=(z1)} \right) \right)}{\tau}$ (51)
$\psi_{0,0}^b(z1, z2)$	$0 = k_{H,CGC} [H_2] \left(\lambda_{0,0}^b \phi_{0,0}^b(z1, z2) \right) + \frac{\left(\left(\mu_{0,0}^b \psi_{0,0}^b(z1, z2) \right)_{\text{feed}} - \left(\mu_{0,0}^b \psi_{0,0}^b(z1, z2) \right) \right)}{\tau}$ (52)
$\psi_0^{\text{lin}}(z1)$	$0 = k_{H,\text{lin}} [H_2] \left(\lambda_0^{\text{lin}} \phi_0^{\text{lin}}(z1) \right) + \frac{\left(\left(\mu_0^{\text{lin}} \psi_0^{\text{lin}}(z1) \right)_{\text{feed}} - \left(\mu_0^{\text{lin}} \psi_0^{\text{lin}}(z1) \right) \right)}{\tau}$ (53)

Table 5. Moment balance equations for a steady-state CSTR.

Moment	Balance Equation
$\lambda_{0,0}^b$	$0 = k_{i,CGC} [M] C_{CGC}^* - (k_{\beta,CGC} + k_{d1,CGC} + k_{M,CGC} [M] + k_{H,CGC} [H_2]) \lambda_{0,0}^b + \frac{\lambda_{0,0,feed}^b - \lambda_{0,0}^b}{\tau} \quad (56)$
λ_0^{lin}	$0 = k_{i,lin} [M] C_{lin}^* - (k_{\beta,lin} + k_{d1,lin} + k_{M,lin} [M] + k_{H,lin} [H_2]) \lambda_0^{\text{lin}} + \frac{\lambda_{0,feed}^{\text{lin}} - \lambda_0^{\text{lin}}}{\tau} \quad (57)$
$\mu_{0,0}^{b=}$	$0 = (k_{\beta,CGC} + k_{d1,CGC} + k_{M,CGC} [M]) \lambda_{0,0}^b - k_{p,TDP} \lambda_{0,0}^b \mu_{0,0}^{b=} + \frac{\mu_{0,0,feed}^{b=} - \mu_{0,0}^{b=}}{\tau} \quad (58)$
$\mu_0^{\text{lin} =}$	$0 = (k_{\beta,lin} + k_{d1,lin} + k_{M,lin} [M]) \lambda_0^{\text{lin}} - k_{p,TDP} \lambda_{0,0}^b \mu_0^{\text{lin} =} + \frac{\mu_{0,feed}^{\text{lin} =} - \mu_0^{\text{lin} =}}{\tau} \quad (59)$
$\mu_{0,0}^b$	$0 = k_{H,CGC} [H_2] \lambda_{0,0}^b + \frac{\mu_{0,0,feed}^b - \mu_{0,0}^b}{\tau} \quad (60)$
μ_0^{lin}	$0 = k_{H,lin} [H_2] \lambda_0^{\text{lin}} + \frac{\mu_{0,feed}^{\text{lin}} - \mu_0^{\text{lin}}}{\tau} \quad (61)$

Table 6. Process operating conditions used in the model simulation (Iedema & Hoefsloot, 2003).

Process variable	Value	Units
$[H_2]$	1.13×10^{-3}	$\text{kmol} \cdot \text{m}^{-3}$
τ	300	s
r_{CGC}	0.8	-
$C_{\text{CGC,feed}}^*$	$4 \times 10^{-6} \cdot r_{\text{CGC}}$	$\text{kmol} \cdot \text{m}^{-3}$
$C_{\text{lin,feed}}^*$	$4 \times 10^{-6} \cdot (1 - r_{\text{CGC}})$	$\text{kmol} \cdot \text{m}^{-3}$
$(\lambda_{0,0}^b \phi_{0,0}^b(z1, z2))_{\text{feed}}, (\lambda_{0,0}^{\text{lin}} \phi_{0,0}^{\text{lin}}(z1))_{\text{feed}},$ $(\mu_{0,0}^{b=} \psi_{0,0}^{b=}(z1, z2))_{\text{feed}}, (\mu_{0,0}^{\text{lin}=} \psi_{0,0}^{\text{lin}=}(z1))_{\text{feed}},$ $(\mu_{0,0}^b \psi_{0,0}^b(z1, z2))_{\text{feed}}, (\mu_{0,0}^{\text{lin}} \psi_{0,0}^{\text{lin}}(z1))_{\text{feed}}, \lambda_{0,0, \text{feed}}^b,$ $\lambda_{0, \text{feed}}^{\text{lin}}, \mu_{0,0, \text{feed}}^{b=}, \mu_{0, \text{feed}}^{\text{lin}=}, \mu_{0,0, \text{feed}}^b, \mu_{0, \text{feed}}^{\text{lin}}$	0	$\text{kmol} \cdot \text{m}^{-3}$

Table A. 1. Actual and theoretical inversion errors using the 2D IFG method with $N_1 = 140$ and $N_2 = 8$ for the analytical distribution $p^1(n, m)$.

n	m	Actual error $(\bar{p}(n, m) - p(n, m))$	Theoretical Error (Eq. (25))
70	1	1.1219E-05	1.1267E-05
80	1	1.8853E-04	1.8858E-04
90	1	9.0836E-04	9.0841E-04
100	1	1.4461E-03	1.4462E-03
110	1	8.4972E-04	8.4977E-04
120	1	2.0170E-04	2.0176E-04
70	3	2.4566E-06	2.5600E-06
80	3	4.2732E-05	4.2847E-05
90	3	2.0628E-04	2.0640E-04
100	3	3.2846E-04	3.2858E-04
110	3	1.9295E-04	1.9308E-04
120	3	4.5726E-05	4.5841E-05
70	5	2.8717E-07	4.1023E-07
80	5	6.7281E-06	6.8660E-06
90	5	3.2923E-05	3.3075E-05
100	5	5.2495E-05	5.2653E-05
110	5	3.0789E-05	3.0939E-05
120	5	7.2078E-06	7.3457E-06
70	6	4.4383E-08	1.4651E-07
80	6	2.3375E-06	2.4521E-06
90	6	1.1686E-05	1.1812E-05
100	6	1.8672E-05	1.8804E-05
110	6	1.0923E-05	1.1050E-05
120	6	2.5087E-06	2.6234E-06